Examining the Effect of Parvalbumin Overexpression on the Development of Centronuclear Myopathy in Phospholamban Overexpressing Mice

by

Mark Andrew Valentim

A thesis

presented to the University of Waterloo

in fulfilment of the

thesis requirement for the degree of

Master of Science

in

Kinesiology

Waterloo, Ontario, Canada, 2022

Author's Declaration

I hereby declare that I am the sole author of this thesis. This is a true copy of the thesis, including any required final reversions, as accepted by my examiners.

I understand that my thesis may be made electronically available to the public.

Abstract

Within the myofibre, the sarco(endo)plasmic reticulum (SR) Ca^{2+} ATPase (SERCA) has an essential role in regulating intracellular Ca^{2+} concentrations ($[Ca^{2+}]_i$) by pumping Ca^{2+} into the SR. There are several known regulators of SERCA, including phospholamban (PLN), an inhibitory protein which binds to SERCA causing a reduction in affinity for Ca^{2+}. Recently, it was discovered that the overexpression of PLN in slow-twitch (type I) muscle fibres results in a disease phenotype resembling centronuclear myopathy (CNM). CNM encompasses a group of diseases which are identified by three main histological characteristics: 1) an increased proportion of centralized nuclei, 2) a centralization of oxidative activity and 3) an increased proportion of type I fibres. Although the pathogenesis of CNM remains unknown, there is evidence that suggests dysfunctional Ca^{2+} homeostasis may be involved. The involvement of dysfunctional Ca^{2+} handling is further supported by the CNM-like phenotype developed in PLN overexpressing mice (PLN^{OE}), as the inhibitory action of PLN increases $[Ca^{2+}]_i$. The purpose of this project was to examine the therapeutic potential of overexpressing the cytosolic Ca^{2+} buffering protein parvalbumin (PV) in PLN^{OE} mice. As a Ca^{2+} buffering protein, PV binds Ca^{2+} when $[Ca^{2+}]_i$ increases allowing for a faster return to resting concentrations. However, evidence reported in this thesis found the transgenic upregulation of PV did not improve the disease phenotype in PLN^{OE} mice. Specifically, the PV intervention did not reduce the percentage of centralized nuclei, the presence of centralized oxidative activity, and shift toward type I fibres. Furthermore, PV did not improve the reduced soleus weight in the diseased tissue, nor did it improve the reduced cross-sectional area observed in the type I fibres. Functionally, the overexpression of PV did not change the rate of Ca^{2+} uptake and did not result in improvements

in force production. The findings of this thesis suggest a PV intervention to sequester excess cytosolic Ca^{2+} may not be feasible in treating CNM.

Acknowledgements

Thank you to my parents. You have always supported me in all my endeavours and encouraged me to put forth my best effort. You are two of the hardest working people I know, and I am so grateful to have you as role models. You have always been there to answer my FaceTime calls when I needed a break from writing and to listen to my presentations even if you had no idea what it was about.

Thank you to my supervisor, Dr Russ Tupling. I have been in your lab for five years and in that time, I have learned so many valuable things from you, not just about the science but also about life. Your positive attitude has always been reassuring, especially when I have felt the pressure of looming deadlines. Your support and flexibility over these past two years has been very helpful, particularly when dealing with the various pandemic-related hurdles. I look forward learning and growing with you as my supervisor in the coming years.

To my lab mates: Emma Juracic, Paige Chambers, Adi Brahmbhatt and Elizabeth Labonte – you have made these last two years special. Emma and Paige, thank you for always being there for the many questions I had in lab. Additionally, thank you to all the other Kin physiology students especially Ashkan Hashemi, Megan Lo, Joey Hung and John Chan. Talking with all of you on the fourth floor almost always left me laughing. The long days in lab would not have been the same without the midday walks to Tim Horton's and the post lab workouts over at CIF. It has been a pleasure working alongside each of you.

Table of Contents

List of Figures

List of Tables

List of Abbreviations

Ca^{2+} – Calcium
$[Ca^{2+}]$ – Intracellular Calcium
CaM – Calmodulin
CnA – Calcinuerin
CNM – Cen
tronuclear Myopathy
CSA – Cross-Sectional Area
DB^{OE} – Double Overexpressing Group
DHPR – Dyhydropyridine Receptor
MHC – Myosin Heavy Chain
NFAT – Nucelar Factor of Activated T Cells
PLN – Phospholamban
PLN^{OE} – Phospholamban Overexpressing Group
PV – Parvalbumin
PV^{OE} – Parvalbumin Overexpressing Group
ROS – Reactive Oxygen Species
RNS – Reactive Nitrogen Species
SR – Sarcoplasmic Reticulum
SERCA – Sarco(endo)plasmic Reticulum Calcium ATPase
TnC – Troponin C

Introduction

Calcium and Muscle Homeostasis

Within the body, calcium (Ca^{2+}) exists as a divalent cation with chemical properties which allow it to form abnormal ligation geometries when binding with intracellular molecules. The binding coordination of Ca^{2+} is essential for precise control of its concentration making it an ideal second messenger (Carafoli & Krebs, 2016). Within the skeletal muscle, Ca^{2+} is involved in various intracellular pathways to promote healthy muscle function both acutely, during excitation contraction coupling, and chronically through regulating gene expression.

Under resting conditions in skeletal muscle, high concentrations of Ca^{2+} are sequestered within the sarcoplasmic reticulum (SR). The SR is a network of membranous tubules surrounding the filamentous contractile proteins that make up the sarcomere (Sommer, 1982). Within the lumen of the SR exists the buffering protein calsequestrin which further improves Ca^{2+} storage allowing the resting cytosolic [Ca^{2+}] to be maintained below 100nM (Berridge et al., 2000; Schiaffino & Reggiani, 1994). Resting [Ca^{2+}] is maintained until neural signalling depolarizes the sarcolemma, which triggers a conformational change in the voltage sensing dihydropyridine receptor (DHPR) located within the transverse tubule membranes (Dulhunty, 2006). The structural change of the DHPR reduces its interaction with the functionally-linked ryanodine receptor (RyR) inducing the rapid release of Ca^{2+} from the SR (Dulhunty, 2006).

The release of Ca^{2+} acts as an essential signaling molecule in crossbridge cycling. When [Ca^{2+}] rises above 1000nM, Ca^{2+} associates with troponin C (TnC) causing a subsequent structural change in Troponin I resulting in the movement of tropomyosin (Calderón et al., 2014). The movement of tropomyosin exposes the myosin head binding site on the actin molecule allowing the formation of crossbridges (Gordon et al., 2001; Holmes, 2008).

Crossbridge cycling then occurs when ATP hydrolysis drives movement of the myosin heads to slide past actin filaments in a manner which shortens the length of the sarcomere resulting in the development of force (Holmes, 2008).

Calcium and Fibre Type Signaling

Mammalian skeletal muscle is composed of a collection of heterogenous fibre types which arise during embryonic development (Condon et al., 1990; Pette & Staron, 1997). Classification schemes of muscle fibres traditionally involve differentiating fibres through contractile speed, metabolic properties or myosin heavy chain (MHC) isoform expression (Pette & Staron, 1997). In adult mammalian muscles, 4 main MHC isoforms exist: one slow isoform (MHCI) in Type I fibres and three fast isoforms (MHCIIa, MHCIIx, MHCIIb) in Type II fibres (Schiaffino & Reggiani, 1994). For consistency in nomenclature, muscle fibres are named based on the MHC isoform expressed (ie MHCIIa = Type IIA muscle fibre) (Scott et al., 2001). However, fibres may also express more than one MHC isoform at once and thus be considered hybrid fibres.

The existence of hybrid fibres is explained by the innate plasticity of skeletal muscle which can modify gene expression to meet the demands of applied stimuli as well as during diseased states (Burnham et al., 1997; Grossman et al., 1998; Salmons & Vrbova, 1969; Termin et al., 1989). The transition of MHC gene expression follows a well-established, obligatory pathway: I←→I/IIA←→IIA←→IIA/IIX←→IIX←→IIX/IIB←→IIB (Green & Pette, 1997). Previous research has shown that chronic low frequency stimulation, muscle lengthening and mechanical loading result in signaling which promotes shifts towards slower MHC isoforms. (Degens et al., 1995; Pattullo et al., 1992; Termin et al., 1989). In contrast phasic high frequency

stimulation, unload, and denervation signal for a conversion to a fast fibre type gene program (Burnham et al., 1997; Caiozzo et al., 1994; Gundersen et al., 1988; Schiaffino et al., 1988).

Collectively, research has shown that neural signalling influences the fibre type gene expression in muscle. Specifically, studies using cross innervation and electrical stimulation have shown that fibre type gene programming appears to be dependent on the frequency of stimulation of the muscle (Bárány & Close, 1971; Vrbová, 1963). Motor neurons fire at 10-20 Hz and 70-90 Hz in slow and fast muscle fibres respectively (Hennig & Lomo, 1985; Schiaffino & Reggiani, 2011). Additionally comparative studies analyzing continuous motor neuron firing found slow motor neurons can fire continuously for 300-500s, type IIA/IIX for 60-140s and type IIB fibres for < 3s (Schiaffino & Reggiani, 2011). Furthermore, a combination of motor neuron signalling frequency and the different isoforms of Ca^{2+} handling proteins result in different oscillations of $[Ca^{2+}]_i$ between fibre types. Fast muscle fibres experience Ca^{2+} transients with high amplitude spikes which involve faster rates of Ca^{2+} release and reuptake. In contrast , in slow fibres the peak $[Ca^{2+}]_i$ is only about half that of type II fibres but Ca^{2+} oscillations are more phasic, lasting much longer durations (Baylor & Hollingworth, 2003; Schiaffino & Reggiani, 2011). Despite this finding, in rodent muscle, slow fibres have a higher resting $[Ca^{2+}]$ (50-60nM) in comparison to fast fibres (30nM) (Schiaffino & Reggiani, 2011). In summary, $[Ca^{2+}]_i$ amplitudes are highest in faster fibres but are longer lasting in slower fibres.

Differences in the Ca^{2+} concentrations can be differentiated through the calcineurin (CnA) calmodulin (CaM) pathway. CnA is a serine/threonine phosphatase which acts as a bridge between calcium signaling and the phosphorylation states of numerous downstream transcriptional regulators (Klee et al., 1979; Rumi-Masante et al., 2012). CnA is a heterodimeric protein composed of two subunits: a ~60kDa A chain and a 19kDa B chain. The A chain consists

of a regulatory domain which binds CaM, a catalytic domain, and autoinhibitory domain. The B chain is a Ca^{2+} binding domain with an ability to bind 4 calcium ions (Klee et al., 1979; Yang & Klee, 2000). When $[Ca^{2+}]_i$ is low, the CnA is inactive with the autoinhibitory domain bound to the catalytic domain. As the $[Ca^{2+}]$ rises, Ca^{2+} ions will bind to CaM which will allow for the regulatory domain of CnA to bind to CaM. The binding of CaM will result in the autoinhibitory domain to release, thus exposing the CnA catalytic domain (Rumi-Masante et al., 2012). With the catalytic domain exposed, CnA can target downstream transcriptional factors.

Notably, CnA acts as a Ca^{2+} sensor which can signal for the programming of fibre type. With elevations of $[Ca^{2+}]_i$, CnA phosphatase activity increases resulting in more dephosphorylation of myocyte enhancement factor 2 and the nuclear factor of activated T cells (NFAT) family of transcription factors (NFATc1-4 and NFAT5) (Carpenter, 2001; Rao et al., 1997). With sufficient phosphatase activity, dephosphorylated transcription factors can translocate into the nucleus and influence the fibre type gene program.

Previous research has found that CnA activity signals for a slow fibre type gene program. When transgenic mice express CnA with increased activity it caused an increased percentage of type I fibres (Chin et al., 1998; Naya et al., 2000). In contrast, mice exposed to the CnA inhibitors cyclosporin A and FK506 display a shift towards a type II phenotype (Chin et al., 1998; Dunn et al., 1999; Serrano et al., 2001). Furthermore NFATc1 appears to be directly involved with fibre type transitions as research involving constitutively active NFATc1 in rat skeletal muscle resulted in increased MHCI expression while expression of MHCIIx and MHCIIb were repressed (Chakkalakal et al., 2003; McCullagh et al., 2004).

Sarco(Endo)plasmic Reticulum Ca^{2+} ATPase

SERCA is a P-Type divalent cation dependent ATPase. With a molecular mass of 110 kDa, SERCA is a single polypeptide molecule embedded in the membrane of the SR and endoplasmic reticulum (MacLennan et al., 1985). Structurally, SERCA is composed 3 cytoplasmic domains: (Phosphorylation(P-), Actuator (A-) and Nucleotide (N-domains)); and 10 transmembrane helices (M1- M10) (Toyoshima et al., 2000). Within these transmembrane helices exist two Ca^{2+} binding sites which are only accessible for binding by cytoplasmic Ca^{2+}. Three isoforms (SERCA1, SERCA 2 and SERCA3) have been identified which arise from the genes ATP2A1, ATP2A2 and ATP3A3 respectively (Brandl et al., 1986, 1987; Periasamy & Kalyanasundaram, 2007). Further variants in the three SERCA isoforms are attributable to alternative splicing (Brandl et al., 1986, 1987; Periasamy & Kalyanasundaram, 2007). Within skeletal muscle, SERCA1a is expressed in adult type II fibres and SERCA2a is expressed in type I fibres (Brandl et al., 1987; Periasamy & Kalyanasundaram, 2007).

Like other P-type ATPases, SERCA undergoes drastic conformational changes with the binding of cations and ATP. Generally, through the cycle of Ca^{2+} pumping, SERCA alternates between an E1 and E2 state. In the E1 conformation, Ca^{2+} binding sites are accessible by cytosolic Ca^{2+}. While still in the E1 configuration ATP binds to SERCA is such a way that the adenine residue is bound to the N-domain and the gamma phosphoryl residue is bound to the P-domain (Haviv & Karlish, 2013). Along with the ATP molecule, a Mg^{2+} binds to the P-domain causing it to become bent. The binding of the ATP molecule causes a change to the shape of the SERCA molecule resulting in the M1 helix being pulled up and bent in such away which closes the cytosolic opening thus making it impossible for Ca^{2+} to move into the cytosol. As ATP hydrolysis occurs the gamma phosphate is transferred on to Asp 351 which triggers a separation

of the N and P- domains while also causing a rotation of the A-domain (Toyoshima & Inesi, 2004). The separation of the N and P- domains is the major characteristic of a shift from an E1-phosphorylated state to an E2- phosphorylated state. The change in shape of the domains in the cytosolic head are translated into conformational changes in the transmembrane helices. Specifically, helices M1-M6 have large movements around the Ca^{2+} binding sites essentially diminishing the affinity needed for Ca^{2+} binding. Furthermore, movement of M1 and M2 push against the M4 helix resulting in the opening of the SR luminal gate, allowing Ca^{2+} to disassociate into the SR. Then, with the use of a water molecule, the A-domain catalyzes and attack on the aspartylphosphate on the N-domain causing the release of a phosphate and Mg^{2+} (Haviv & Karlish, 2013). The removal of phosphate and Mg^{2+} from the P-domain allows this domain to re-establish an unbent conformation and thus closes the luminal gate. Lastly, the E2 conformation reverses back into E1 thus reopening the cytosolic gate to allow new cytosolic Ca^{2+} access to the Ca^{2+} binding sites (Haviv & Karlish, 2013).

Phospholamban

Research has identified several proteins which act to regulate SERCA function either positively or negatively (Anderson et al., 2016; Fajardo et al., 2013; Makarewich et al., 2018). Among these SERCA regulators, phospholamban (PLN) is one of the most studied due to its inhibitory properties which have been implicated in various forms of cardiomyopathy (Kranias & Hajjar, 2012). PLN is expressed in both the atria and the ventricles of the heart and in skeletal muscle (Minamisawa et al., 2003). Specifically within skeletal muscle, PLN has been detected in both type I and type II fibres but appears to be expressed in greater quantities in fibres expressing MHCI (Damiani et al., 2000; Fajardo et al., 2013).

PLN is a 52 amino acid protein located in the SR membrane where it can interact with SERCA (Gorski et al., 2013). PLN is composed of a small luminal domain, a transmembranous domain and a cytosolic domain (Gorski et al., 2013). The transmembranous domain consists of a single helix which can directly bind to the Ca^{2+} binding site formed by the M2, M4, M6 and M9 helices of SERCA (Hutter et al., 2002; Toyoshima et al., 2003). In binding to SERCA, PLN elicits an inhibitory effect on the Ca^{2+} pump by reducing the apparent affinity of Ca^{2+} binding (Asahi et al., 2003; Gorski et al., 2013). Although research has shown that PLN reduces Ca^{2+} affinity to SERCA, its role at maximal $[Ca^{2+}]_i$ is less clear as increases in $[Ca^{2+}]_i$ can cause PLN dissociation from SERCA (Gorski et al., 2015; Mundiña Weilenmann et al., 2005). Additionally, research has found that PLN can form a complex with sarcolipin (SLN), another negative regulator of SERCA (Asahi et al., 2002). Together this complex has a superinhibitory effect causing reductions in Ca^{2+} affinity of approximately -1.0 pCa units and significant depressions in maximal SERCA activity (Asahi et al., 2002).

The inhibitory action of PLN on SERCA can be disrupted via phosphorylation of two sites within the cytosolic domain of PLN. These phosphorylation sites are targeted by two different kinases: Ser16 by cAMP dependent protein kinase A (PKA), and Thr17 by Ca^{2+} calmodulin dependent protein kinase II (CAMKII) (MacLennan & Kranias, 2003; Wegener et al., 1989). Upon phosphorylating either of these sites, PLN will dissociate from SERCA and reside within the SR membrane existing in its monomeric form or in homopentameric units (Wegener & Jones, 1984). The exact role of PLN pentamers remains relatively ambiguous with some reports suggesting it acts as a storage site for PLN while other research suggests it may act as a selective cation channel (Smeazzetto et al., 2016; Wittmann et al., 2015).

With respect to muscle health, PLN has long been researched for its role in cardiomyopathy. PLN is naturally expressed in cardiac tissue and has a role in modulating cardiac contractility through its inhibitory effect on SERCA(Kranias & Hajjar, 2012). However, mutations in the amino acid sequence of PLN have been associated with models of cardiomyopathy. Within cardiomyopathy models, mutated PLN can impose greater inhibition of SERCA resulting in decreases in the rate of relaxation and improper ventricular filling (Z. Chen et al., 2007; Kranias & Hajjar, 2012). Mutational studies involving models with reduced PLN function have also been associated with dilated cardiomyopathy (Schmitt et al., 2003). Although there is far less research on PLN and skeletal muscle disease, there are now multiple groups who have found that the overexpression of PLN causes a disease-like phenotype in skeletal muscle (Fajardo et al., 2015; Pattison et al., 2008; Song et al., 2004). Specifically, Fajardo et al. (2015) found that PLN overexpression (PLN^{OE}) mice appear to represent a novel model of centronuclear myopathy (Fajardo et al., 2015).

Centronuclear Myopathy

Centronuclear myopathy (CNM) is a heterogenous group of inherited neuromuscular diseases characterized by increased localization of centralized nuclei. Although variance exists among disease phenotypes, other common histological indicators include an increased proportion of type I fibres, a central aggregation of oxidative activity, and fibrosis (Jungbluth et al., 2008). CNM was originally reported in the mid 1960's in an adolescent boy with reduced distal muscle tone (Spiro et al., 1966). In this report, CNM was referred to as a muscle wasting disease which was postulated to be due to an arrest in myotube development (Spiro et al., 1966). The following year, Sher et al. (1967) described two sisters with a similar disease phenotype but concluded the

affected myofibres differed from fetal myotubes and thus favoured the term “centronuclear myopathy” (Sher et al., 1967). Since then, multiple gene mutations have been identified which have led to the development of a similar disease-phenotype with variations in clinical presentation and disease severity (Jungbluth & Gautel, 2014). Although the mechanisms involved in pathogenesis remain unknown, understanding the CNM associated gene mutations may provide insight into the pathways involved.

Among the CNM diseases, the most severe cases arise in a X-linked inheritance pattern from a mutation in the *MTM1* gene. MTM1-CNM encodes for myotubularin, a phosphoinositide phosphatase responsible for dephosphorylating phosphatidylinositol 3-phosphate [PI(3)P] and phosphatidylinositol 3,5-phosphate (PI(3,5)P) (Jungbluth & Gautel, 2014). Research in multiple experimental models have found that myotubularin functions to regulate PI(3)P, endocytosis and endolysosomal function(Blondeau et al., 2000; Cowling et al., 2012). Furthermore, two sporadic cases with CNM features occur in individuals within the MTMR14 gene, a gene with considerable homology of its catalytic motif to myotubularin (Alonso et al., 2004; Jungbluth & Gautel, 2014). The MTMR14 protein; hJUMPY shares the same catalytic targets of myotubularin (Tosch et al., 2006). Research focused on hJUMPY knockout mice has found that mutant mice have an excessive accumulation of $PI(3,5)P_2$ within the SR membrane which is accompanied by dysfunctional storage of Ca^{2+} within the SR (Shen et al., 2009). Further investigation focused on the open probability of the RyR1 suggests that the increase in PIPs present in the SR membrane may have a role in activating RyR1 at lower $[Ca^{2+}]_i$ and thus causing greater Ca^{2+} leak (Shen et al., 2009). Thus, the function of myotubularin suggests that impaired membrane trafficking and/or abnormal Ca^{2+} handling may be involved with CNM pathogenesis.

Milder cases of CNM have been reported in individuals with a DNM2 autosomal dominant mutation. *DNM2* encodes dynamin 2, a large GTPase protein which drives the fission of membranes by providing constriction around vesiculating necks (Praefcke & McMahon, 2004). It has also been proposed that dynamin 2 may be implicated in microtubule networks, actin cytoskeleton assembly and centrosome cohesion (González-Jamett et al., 2013; Jungbluth & Gautel, 2014). Research by Fraysse et al. (2016), using a Dynamin 2 related CNM mouse model found that the EDL of transgenic mice contained elevated resting $[Ca^{2+}]_i$ (Fraysse et al., 2016). The elevated $[Ca^{2+}]_i$ is suggested to originate from the plasma membrane which had been shown to have increased permeability (Fraysse et al., 2016). Again, similar to a MTM1 mutation, DNM2-CNM appears to involve impairments in Ca^{2+} homeostasis and membrane trafficking.

Another moderately severe form of CNM arises from a *BIN1* mutation (Jungbluth & Gautel, 2014). *BIN1* encodes for amphiphysin-2, a protein involved in pathways associated with the membrane recycling and is regulated by phosphoinositides (Jungbluth & Gautel, 2014; Prokic et al., 2014). Specifically, *BIN1* contains a BAR domain that senses and induces membrane curvature and a C-terminal domain which associates with effectors such as dynamins (Cowling et al., 2017). *BIN1* recessive mutations often impair its membrane tubulation properties, its ability to interact with dynamin 2 or the phosphoinositide-binding domain (Cowling et al., 2017). Abnormalities in triad and t-tubule formation found in *BIN1* deficient zebrafish resemble a similar phenotype observed in *MTM1* and *DNM2* CNM suggesting a shared pathway may be involved in CNM pathogenesis (Jungbluth & Gautel, 2014).

Further evidence for a shared pathway by *MTM1*, *DNM2* and *BIN1* has been observed by Cowling et al who have characterized relationships between these genes by manipulating protein

expression (Cowling et al., 2014). In 2014, Cowling et al discovered that reducing dynamin 2 expression rescues mice with *MTM1*-CNM (Cowling et al., 2014). Later it was also reported that amphiphysin-2 is negatively regulated by dynamin 2 in vitro and in vivo (Cowling et al., 2017). Interestingly, forms of CNM involving mutations in *MTM1*, *DNM2* and *BIN1* have all had been associated with improper triad assembly and function (Jungbluth & Gautel, 2014). Although myotubularin, dynamin 2 and amphiphysin-2 function as membrane trafficking proteins, mutations of these proteins have been associated with Ca^{2+} dysregulation (Caldwell et al., 2014; Fraysse et al., 2016; Kutchukian et al., 2019).

Recently, mutations in *RYR1* and *TTN*, the genes encoding skeletal muscle RyR and the cytoskeletal protein titin, respectively, have also been implicated in the development of a CNM phenotype providing greater evidence for the involvement of Ca^{2+} in CNM pathogenesis (Ceyhan-Birsoy et al., 2013; Wilmshurst et al., 2010). RyR1 related CNM differs from other forms of CNM as there appears to be no direct links to defective membrane trafficking (Jungbluth & Gautel, 2014). *RyR1* gene mutations are heterogeneous and can involve substitution of conserved residues, and improper truncation (Bevilacqua et al., 2011). CNM cases involving RyR1 truncations have been shown to result in a down-regulation of RyR1, as well as a secondary reduction in the DHPR content, an increase in IP_3 receptors and improper triad formation (H. Zhou et al., 2013). Mutations to *TTN* which cause CNM also remain relatively heterogenous; however, most appear to involve C-terminus truncations (Jungbluth & Gautel, 2014). Mutations affecting the Titin C-terminus are associated with a reduction in calpain-3 and nebulin-2, two proteins which interact with the C-terminal region (Ceyhan-Birsoy et al., 2013; Jungbluth & Gautel, 2014). Previous work has shown that calpain-3 has a role in maintaining the structural integrity of the triad allowing for proper formation of Ca^{2+} release channels

(Kramerova et al., 2008). When a mutation occurs in the *TTN* C-terminal region, calpain-3 expression is reduced which may cause irregularities in Ca^{2+} release (Jungbluth & Gautel, 2014; Kramerova et al., 2008).

Although the pathogenic mechanisms of CNM remain unknown, previous evidence suggests dysfunctional Ca^{2+} homeostasis may be involved. It is yet to be determined whether abnormal Ca^{2+} handling has a role in initiating pathogenesis or is just a consequence of upstream dysfunction. Ca^{2+} is integrated into many intracellular pathways and if Ca^{2+} handling is disrupted by upstream mechanisms it may exacerbate the myopathic phenotype. For example, elevated $[Ca^{2+}]_i$ can result in the activation of calpains and caspases leading to greater protein degradation (Sanvicens et al., 2004). Additionally, amplified $[Ca^{2+}]_i$ can also result in oxidative stress and mitochondrial swelling (Lemasters et al., 2009).This can result in a positive feedback loop as previous work has shown that SERCA is susceptible to reactive oxygen species (ROS) and reactive nitrogen species (RNS) damage (Dremina et al., 2007). ROS and RNS damage to SERCA can make it ineffective in transporting Ca^{2+} resulting in a reduced capacity to clear $[Ca^{2+}]_i$ (Dremina et al., 2007). Consequently, reduced $[Ca^{2+}]_i$ clearance would further augment calpain/caspase activation and increase the presence of ROS/RNS. Furthermore increased $[Ca^{2+}]_i$ can also activate CnA Calmodulin complex which may explain the fibre type shift commonly observed in CNM (Chin et al., 2003). Additional evidence for the role of impaired Ca^{2+} homeostasis in the pathogenesis of CNM comes from the disease appearance with PLN overexpression (Fajardo et al., 2015; Song et al., 2004).

While trying to characterize the role of PLN in SERCA regulation, Song and colleagues (Song et al., 2004) discovered that upregulating the expression of PLN results in muscle disease which was later recognized as a CNM-like phenotype (Fajardo et al., 2015). This novel genetic

form of CNM, which has been observed in an animal model, provides more evidence to support the notion that impaired Ca^{2+} sequestration has a role in initiating CNM pathogenesis. Interestingly, Fajardo and colleagues reported trends for an elevated expression of PLN in human patients diagnosed with CNM (Fajardo et al., 2015). Transgenic models overexpressing PLN have been created in mouse and rabbit models previously (Pattison et al., 2008; Song et al., 2004). Although both models showed signs of myopathy, the disease phenotype remained unclear. However, Fajardo et al. (2015) determined that mice with upregulated PLN displayed an increased centralization of nuclei and oxidative activity as well as type I fibre hypotrophy at 1 month of age (Fajardo et al., 2015). Furthermore, a fibre type shift toward type I fibres was evident by 4-6 months (Fajardo et al., 2015). Interestingly, in this model, the *Pln* transgene is attached to the β-MHC promoter so that these mice overexpress PLN in their slow-twitch type I skeletal muscle fibres and as result the shift to type I fibres would lead to greater expression of PLN causing greater disease severity. In this model, there is also atrophy of type I fibres while there appears to be a compensatory hypertrophy in type II fibres (Fajardo et al., 2015). As a result of histological analysis it was indicated by Fajardo and colleagues that similarities in oxidative staining and fibrosis make PLN^{OE}-related CNM resemble a phenotype which appears more closely related to TTN- and RyR-CNM (Fajardo et al., 2015). The PLN^{OE}-CNM disease model suggests increased $[Ca^{2+}]_i$ may have a role in CNM pathogenesis.

Previous work in our lab has examined different therapeutic approaches for PLN^{OE}-CNM. One approach involved the administration of cyclosporin A to inhibit CnA activity (Chambers, unpublished). The CnA-Ca^{2+} pathway is believed to be involved in the increased proportion of type I fibres and thus it was reasoned that by reducing the fibre type shift, the number of affected fibres overexpressing PLN would be reduced. As expected, cyclosporin A

reduced CnA activity, reduced fibrosis and improved force per cross sectional area in 4-6 month old mice; however, there were no improvements in the proportion of centralized nuclei (Chambers, unpublished). In other unpublished work from our lab, the β-adrenergic agonist formoterol was administered to promote PLN phosphorylation and therefore relieve its inhibitory action on SERCA. In PLN^{OE}-CNM mice, formoterol reduced the proportion of centralized nuclei and fibrosis but centralized oxidative activity was still observed (Rietze, unpublished). The improvement of CNM by reducing the action of PLN on SERCA suggests that the inability to sequester Ca^{2+} could be pathogenic. Therefore, another potential treatment for CNM could involve improving cytosolic Ca^{2+} buffering.

Parvalbumin

Parvalbumin (PV) is a Ca^{2+} buffering protein which has a role in lowering $[Ca^{2+}]_i$ (Heizmann, 1984; Schwaller et al., 1999). Within small mammalian animal models such as mice and rats, PV has been found in neural tissue and type II muscle fibres (Ecob-Prince & Leberer, 1989). In contrast, little or no parvalbumin is expressed in cardiac and type I muscle fibres (Ecob-Prince & Leberer, 1989; Heizmann, 1984; Schwaller et al., 1999). Furthermore, PV has not been detected in human skeletal muscle (Fohr et al., 1993). PV is a 12kDa protein which is expressed in greater quantities in type II fibres than in type I (Fuchtbauer et al., 1991). PV binds Ca^{2+} at an optimal ratio of 2 mol Ca^{2+}: 1 mol parvalbumin (Kretsinger & Nockolds, 1973). These two high affinity binding sites are occupied by Mg^{2+} at resting $[Ca^{2+}]_i$ (<100nM) (Haiech et al., 1979). The rate at which PV can act to sequester Ca^{2+} is dependent on the rate of dissociation of Mg^{2+} from the two PV binding sites (Hou et al., 1991; Schwaller et al., 1999). Consequently, PV buffering does not occur immediately following rises in $[Ca^{2+}]_i$; which is why it is often

considered a slow Ca^{2+} buffer. These binding kinetics of PV explain why its increased expression has been shown to reduce ½ relaxation time and increase the rate of relaxation (-df/dt) while single twitch contractile properties were not attenuated (G. Chen et al., 2001; Chin et al., 2003; Müntener et al., 1995; Schmidt et al., 2005; Schwaller et al., 1999). However during low frequency stimulation of type I fibres, PV overexpression attenuates force production at lower frequencies (30 and 50 Hz) (Chin et al., 2003). Taken together, this research provides evidence that PV is a Ca^{2+} buffering protein which can increase rates of Ca^{2+} sequestration during excitation contraction coupling.

As discussed previously, Ca^{2+} is a known second messenger which can affect fibre type signalling pathways. Given that PV has a role in sequestering $[Ca^{2+}]_i$, it is possible PV may have a role in fibre type signalling. Studies which have focused on the effect of PV on fibre type expression found PV does not result in changes to MHC expression (Chin et al., 2003; Racay et al., 2006; Schmidt et al., 2005). However, research has found that PV overexpression results in an increase in MHCII and RyR mRNA (Chin et al., 2003; Racay et al., 2006; Schmidt et al., 2005). Furthermore, PV knockout animal models have been shown to have an increase in mitochondrial biogenesis and increased capillary density suggesting the absence of PV promotes a more oxidative phenotype (G. Chen et al., 2001; Racay et al., 2006). Chin et al have also reported PV overexpression results in a 64% reduction in calcineurin activity (Chin et al., 2003). Although PV does not appear to exert significant differences in MHC expression, given the other notable changes in mitochondria and capillarization it may still have a role in affecting the CnA-Ca^{2+} pathway through $[Ca^{2+}]_i$ buffering. Through buffering $[Ca^{2+}]_i$, PV may be able to attenuate disease progression by reducing the fibre type shift, reducing the activation of Ca^{2+} sensitive proteolytic enzymes and reduce oxidative stress brought on by elevated $[Ca^{2+}]_i$.

Rationale

PLN^{OE} results in a CNM-like phenotype which is believed to be caused by increased $[Ca^{2+}]_i$. Elevated Ca^{2+} also signals for a shift toward type I fibres which naturally express higher concentrations of PLN. Additionally, the PLN^{OE} transgene is tied to the MHCI promoter, thus increased expression of MHCI results in a greater expression of PLN. This disease model appears to involve a deleterious cycle in which increased PLN causes a shift to type I fibres which further increases PLN expression.

In this PLN^{OE}-CNM model, PV may be able to decrease elevated $[Ca^{2+}]_i$ which could reduce the activation of proteolytic enzymes and oxidative stress thus reducing the disease severity.

Statement of Problem

To date the pathways involved with the development of CNM remain unclear. Although the predominant genetic mutations which cause CNM are linked to membrane trafficking, altered Ca^{2+} dynamics may play a role in disease progression. Recently, it has been shown that the overexpression of the SERCA regulator PLN causes a CNM-like phenotype in mice. This finding would suggest that dysfunctional Ca^{2+} cycling may affect the same pathway involved in the pathogenesis of this myopathy. This thesis will focus on attenuating the progression and severity the CNM by lowering $[Ca^{2+}]_i$ through the overexpression of PV.

Objectives

1. To assess the effect PV overexpression will have on the contractile function and Ca^{2+} uptake in the soleus of PLN^{OE} mice.
2. To assess whether PV overexpression can attenuate muscle atrophy in the soleus of PLN^{OE} mice.
3. To determine whether PV overexpression can reduce the percentage of centralized nuclei, reduce fibrosis and reduce central aggregations of oxidative activity in the muscle of PLN^{OE} mice.
4. To determine is PV overexpression will affect the fibre type shift observed in PLN^{OE} mice.

Hypotheses

1. PV overexpression will improve the force production, contractile properties, relaxation properties and Ca^{2+} uptake in the PLN^{OE} mice.
2. PV overexpression will reduce muscle atrophy in the soleus of PLN^{OE} mice
3. PV overexpression will reduce centralized nuclei, fibrosis, and central aggregations of oxidative activity brought on by PLN^{OE}.
4. PV overexpression will attenuate the shift to type I fibre predominance in PLN^{OE} mice.

Methods

Animals

Four experimental groups were used for this project: a wildtype (WT) group, a parvalbumin overexpressing (PV^{OE}) group, a phospholamban overexpressing (PLN^{OE}) group and a double PLN and PV overexpressing (DB^{OE}) group.

PLN^{OE} mice were originally generated by Song et al. (Song et al., 2004). PLN cDNA was generated by a transgenic fragment then ligated with the ß-MHC promoter. These mice were then made commercially available (000067-MU, Mutant Mouse Regional Resource Centre, Columbia, MO) and were purchased to generate a colony at the University of Waterloo. The transgenic mice originally purchased on a FVB/N background were resuscitated from cryopreserved embryos by the mmRRC (000067-MU) and backcrossed against a C57BL/J6 background for 6 generations. Breeding pairs for colony maintenance involved a heterozygous male with the PLN^{OE} transgene WT female. To assess genotype, ear notch samples were collected, digested, and then amplified through PCR. Details involving the genotyping protocol are listed in appendix A.

PV^{OE} mice on a CD1 background were generated by overexpression of a rat PV cDNA driven by the human troponin I slow promoter (Chin et al., 2003). PV^{OE} mice were attained from the laboratory of Dr. Robin Michel at Concordia University, then crossed with PLN^{OE} mice at the University of Waterloo, creating a line with the potential for progeny which overexpress both proteins. This line remains a mix between C57BL/J6 and CD1 backgrounds.

Maintaining this DB^{OE} colony involves breeding heterozygous male for the $PLN^{OE\ +/-}$ /$PV^{OE-/-}$ transgene and a heterozygous female for the $PV^{OE+/-}$ /$PLN^{OE\ -/-}$ transgene. To assess

genotype, ear notch samples were collected, digested, and then amplified with PCR. Details involving the genotyping protocol are listed in appendix A.

Experimental animals were housed with their sex-matched littermates. Mice were kept in an environmentally controlled room under a reverse light/dark cycle (12/12hr) and were provided access to food and water ad libitum. Tissue collection involved animal sacrifice via cervical dislocation followed by muscle tissue excision. Soleus tissue was isolated from adult mice 4-6 months old. Soleus tissue used for contractility measures were placed directly into an oxygenated bath. Following contractility, tissue samples were mounted in O.C.T compound (Tissue-Tek) and frozen in isopentane cooled by liquid nitrogen for histological analysis. Other soleus tissue was detendonized before being weighed and homogenized in a 1:10 weight to volume dilution in homogenizing buffer (250 mM sucrose, 5mM HEPES, 0.2mM PMSF and 0.2% [w/v] NaN_3). All experiments performed for this thesis were reviewed by the University of Waterloo Animal Care Committee in accordance with the Canadian Council on Animal Care.

Contractility

Immediately following cervical dislocation, intact solei were isolated, removed, and placed directly into an oxygenated bath (95% O_2, 5% CO_2) with Tyrode Solution containing 121 mM $NaCl_2$, 5mM KCl, 24mM $NaHCO_3$, 1.8 mM $CaCl_2$, 0.4mM NaH_2PO_4, 5.5mM glucose, 0.1mM EDTA, and 0.5mM $MgCl_2$, pH =7.3, and will be maintained at 25°C. Muscles were mounted between two platinum electrodes and force will electrically induced at 1, 5 and multiples of 10 until 100Hz using a biphasic stimulator (Model 710B, Aurora Scientific, Inc). Upon the completion of the stimulation protocol, solei were removed and weighed to be used for the normalization of force data. Across all stimulation frequencies, peak isometric force,

maximal rate of contraction and maximal rate of relaxation were recorded. Force was normalized to muscle weight.

Ca^{2+} Uptake

SR Ca^{2+} uptake in muscle homogenates was determined in the presence of a precipitating anion, oxalate. Using the fluorescence dye Indo-1 as previously described (Duhamel et al., 2007). A monochromator maintained an excitation wavelength of 355nm while two photomultiplier tubes detected light emissions at 405 nm and 485 nm. Ca^{2+} uptake was measured in a mixture containing 80uL soleus muscle homogenate, 1879 µL Uptake Buffer (200mM KCl, 20mM HEPES, 10mM NaN_3, TPEN 5mM, 15mM $MgCl_2$, Oxalate 5mM), 40 µL ATP, 1 µL and 1 µL of Indo1. During the assay, EGTA and high Ca^{2+} (100mM) were added to calibrate indo-1 and rates of Ca^{2+} uptake were measured through detecting changes in free Ca^{2+} using indo-1.

Western Blotting

Western blotting for protein quantification was conducted on the following proteins: SERCA1a, SERCA2a, PV, CnA, PLN, NFAT, and pNFAT. Soleus muscle homogenates were normalized with a bicinchonicic acid assay before becoming solubilized in 1X Laemmli buffer (0.1% 2-mercaptoethanol, 0.0005% bromophenol blue, 10% Glycerol, 2% SDS and 63% mM Tris HCl (pH=6.8). Samples were loaded into either tris or glycine based SDS-polyacrylamide gels (Appendix A). All gels were loaded with equal amounts of proteins from all four groups except for the PLN gel. Due to the high expression in the PLN in the PLN^{OE} and DB^{OE} animals, 5 ug of sample was loaded for these groups while 20 ug was loaded for the WT and PV^{OE} groups. Loaded samples underwent electrophoresis for 75 min between 100 and 120V. Then

proteins were transferred to a polyvinylidene difluoride (SERCA1a, SERCA2a, pNFAT, NFAT, CnA, pPLN, PLN, PV; 0.2µm pore size) membrane for a wet transfer at 100V for 60mins (SERCA2a, pNFAT, NFAT, CnA, pPLN, PLN, PV) or 45 mins at 23V using a semi-dry transfer (SERCA1a). Blocking was then conducted with 5% milk in TBST (SERCA1a, SERCA2a, NFAT, CnA, PLN, PV) or BSA (pNFAT, pPLN) overnight at 4°C. Membranes were then washed three times with TBST buffer in increments of 5 mins. Subsequently proteins were immunoprobed with secondary antibody (described in Appendix A). Again, membranes were washed three times with TBST buffer (20 mM Tris base, 137 mM NaCl and 0.1% (v/v) Tween 20, pH 7.5 with 5% [w/v] non-fat dry milk) in 5 min increments. Prior to imaging Luminata Forte™ (SERCA1a, SERCA2a, pPLN, PLN, PV, pNFAT, NFAT) or SuperSignal West Femto™ (CnA) were applied to the membrane to trigger chemiluminescence through horseradish peroxidase. A Chemi Genius Bio Imaging System (Syngene, MD, USA) was used to image and analyze the optical densities. The molecular weights at which bands for each protein were quantified is including in the appendix A. Specifically, the PV transgene contained an -HA tag. As a result transgenic PV (PVHA) was measured at 16 kDa while endogenous PV was assessed at 14 kDa. Following imaging, Ponceau dye was applied to the membrane for 30 minutes and washed by 5% acetic acid for 10 minutes. Membranes were left to dry overnight and were imaged again the following day. A comprehensive list of details for all primary antibodies and protein can be found in appendix A.

Histology

Excised soleus muscles were mounted in O.C.T compound (Tissue-Tek) and frozen in isopentane cooled by liquid nitrogen. Using a cryostat maintained at 20°C, serial cross sections

of 10um thickness were cut and mounted onto slides. These cross sections were then used for Hemotoxylin and Eosin (H&E) staining, Succinate Dehydrogenase (SDH) staining and Van Geison staining. H&E staining was used to determine the positioning of nuclei within the muscle fibre to quantify the percentage of centralized nuclei. SDH staining was used to visualize the localization of oxidative activity. Van Geison staining was used to quantify the proportion of fibrosis. A brightfield Nikon microscope linked to a PixeLink digital camera was used to capture images of stained cross sections. Images were stitched before being analyzed using ImageJ software.

Immunofluorescence

Immunofluorescence analysis was used to assess fibre type distributions in cross sections of collected soleus muscles. The Immunofluorescence protocol used was established by Bloemberg & Quadrilatero, 2012 using primary antibodies against MHCI, MHCIIa, and MHCIIb (antibodies listed in Appendix A) (Bloemberg & Quadrilatero, 2012). Images were collected using AxioCam HRm hardware and AxioVision Software. Images were stitched and analyzed using ImageJ software.

Statistics

All data were presented as mean $\pm$ standard error of the mean (SEM). Most analyses were conducted using either a one-way ANOVA with a Tukey's post-hoc test or a Kruskal-Wallis test with a Dunn test. Contractility measurements were analyzed using a two-way ANOVA comparing groups and frequency. Statistical significance was established at a p-value <0.05. Comparisons considered to be trending toward statistical significance involved p-values < 0.1. R

Statistical Software was used for statistical analysis and GraphPad Prism was used for graphical representation of data.

Results

Animal Physical Characteristics

Adult mice aged 4-6 months with a genotypic background of either WT, PLN^{OE}, PV^{OE}, or DB^{OE} were weighed following sacrifice. Following whole body weight measurements, soleus muscle was excised, detendonized, and weighed. The mean soleus weight of the PLN^{OE} mice ($p<0.05$) and DB^{OE} mice ($p<0.05$) were significantly lower than WT (Fig. 1A). Additionally, the mean soleus weight of the PLN^{OE} ($p<0.05$) and DB^{OE} ($p<0.05$) mice were significantly lower than the PV^{OE} mice (Fig. 1A). Furthermore, when normalizing soleus weights to body weight a similar trend was observed. In comparison to WT mice, PLN^{OE} ($p<0.05$) mice and DB^{OE} ($p<0.05$) mice had a significantly lower normalized soleus weight (Fig. 1B). Similarly, the mean normalized soleus weight was lower in PLN^{OE} ($p<0.05$) mice and DB^{OE} ($p<0.05$) mice when compared to the PV^{OE} mice (Fig. 1B). There were no differences ($p>0.05$) in mean soleus weight or normalized soleus weight between WT and PV^{OE} mice or between PLN^{OE} and DB^{OE} mice.

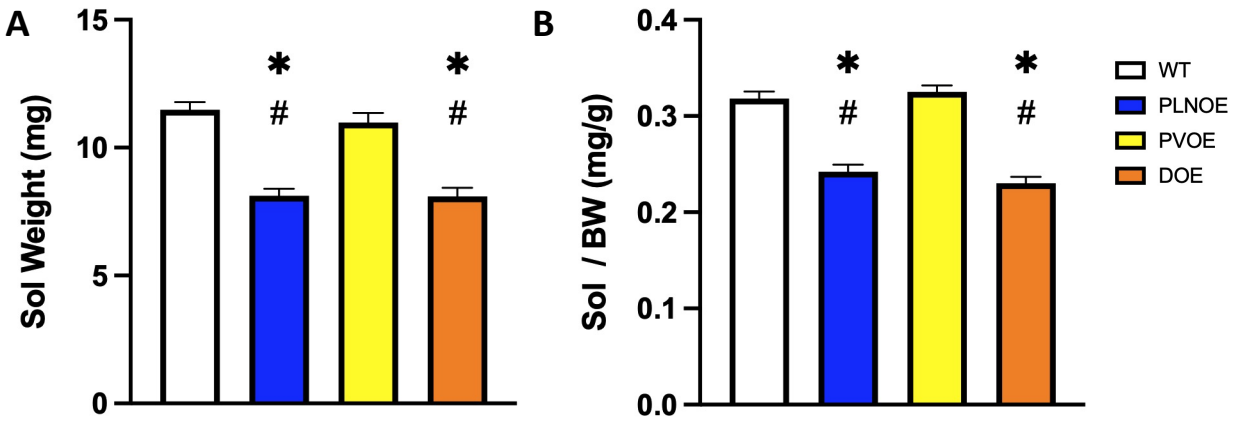

Figure 1: Soleus Weight and Soleus weight Normalized to Body Weight. (A) Mean soleus weight and (B) soleus weight normalized to body weight in WT (n=23), PLN^{OE} (n=17), PV^{OE} (n=18), and DB^{OE} (n=18). * indicates a significant difference from WT ($p<0.05$) and # indicates a significant difference from PV^{OE} ($p<0.05$).

Contractility

Intact soleus muscles from each group were excised and exposed to *ex-vivo* stimulation as described in "Methods". Muscles were stimulated at frequencies ranging from 1-100 Hz to assess contractile and relaxation properties between groups. The visual representation of force generation between groups appears to show a reduced force production at frequencies of 60 Hz and above among groups overexpressing the PLN transgene. However, force production was not statistically different at any given stimulation frequency (Fig. 2A). The rate of relaxation was depressed in DB^{OE} mice in comparison to WT mice at 40Hz ($p<0.05$). Furthermore, at frequencies of 50 Hz and greater there appeared to be a depression in the rate of relaxation in the groups overexpressing PLN. However, statistical analysis revealed these results were only trending toward significance between DB^{OE} and WT mice at 50 Hz ($p=0.066$). All other comparisons of the rate of relaxation between genotypes were not significant (Fig. 2B). Furthermore, there were no statistically significant differences in the contraction rate among the WT, PLN^{OE}, PV^{OE} and DB^{OE} mice across all frequencies (Fig. 2C). Time to peak tension was analyzed during twitch (Fig. 2D) and during 100 Hz stimulation (Fig. 2E). Both measures of time to peak tension found no statistically significant differences ($p>0.05$) among the four groups. Like time to peak tension, half relaxation time was assessed during a single twitch and during 100 Hz stimulation. No significant differences ($p>0.05$) in half relaxation time were found at either stimulation frequency among the four genotypes.

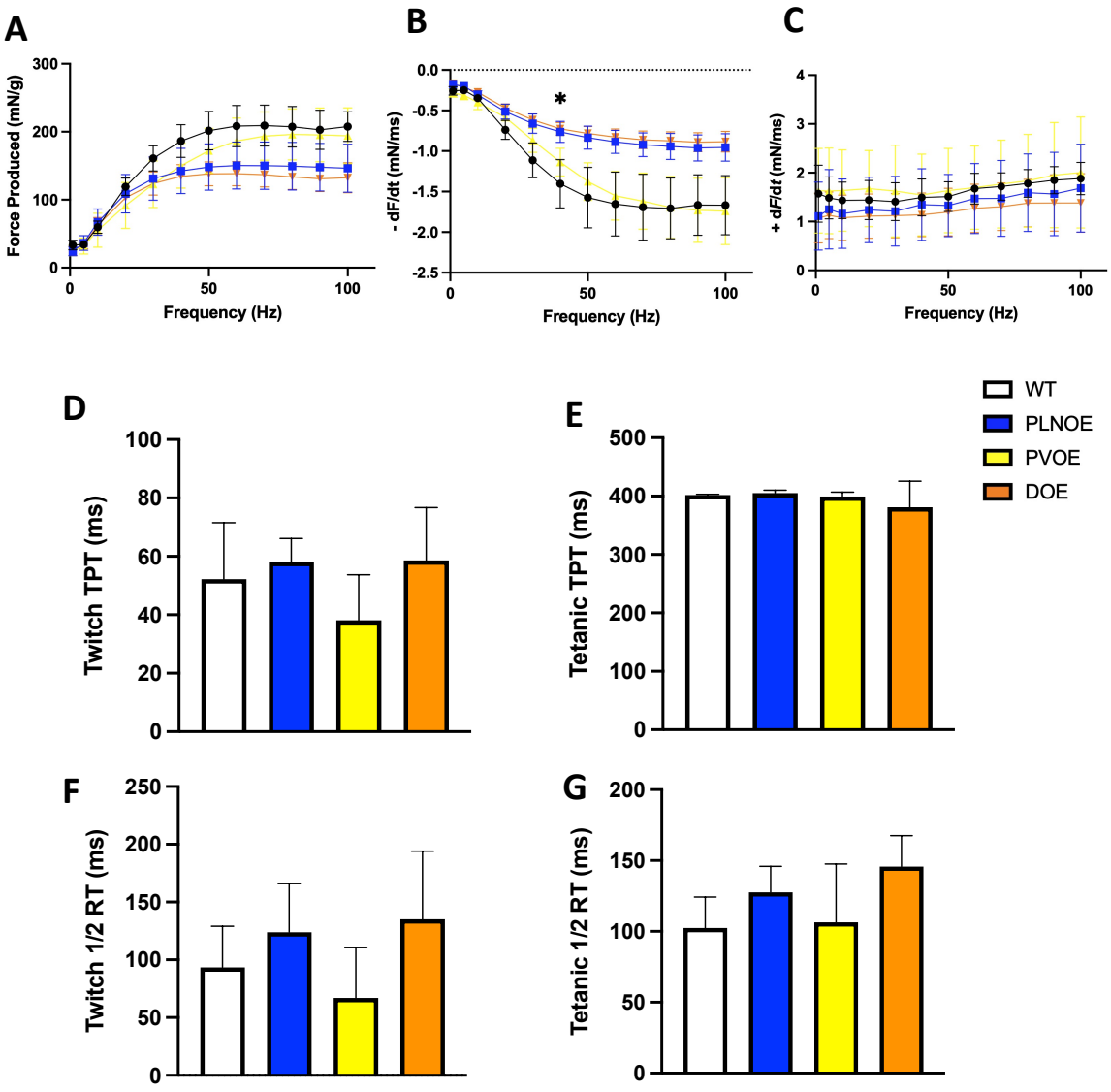

Figure 2: Skeletal Muscle Function Analysis Assessing the Effect of Parvalbumin Overexpression.
(A) Force frequency curves normalized to soleus mass, demonstrating no differences between WT (n= 4), PLN^{OE} (n=4), PV^{OE} (n=4) and DB^{OE} (n=6). (B) The rate of relaxation was attenuated in DB^{OE} mice compared WT mice at 40 Hz. No differences among genotypes when measuring rate of contraction (C), time to peak tension during a muscle twitch (D), time to peak tension when exposed to a 100 Hz stimulation (E), half relaxation time following a muscle twitch (F), and half relaxation time following stimulation at 100 Hz; * indicates a significant difference ($p<0.05$).

Centronuclear Myopathy Features

Histological staining was used to assess the myopathy progression. H&E staining was used to visualize the position of the nuclei. Myofibres with nuclei positioned centrally were quantified and expressed as a percentage of total amount of myofibres (Fig. 3A). The percentage in soleus tissue was significantly higher in the PLN^{OE} tissue and DB^{OE} tissue in comparison to WT ($p<0.05$, $p<0.05$respectively) and in comparison, with PV^{OE} ($p<0.05$, $p<0.05$ respectively). There were no differences observed between PLN^{OE} and DB^{OE} samples ($p > 0.05$ or between WT and PVOE ($p > 0.05$).

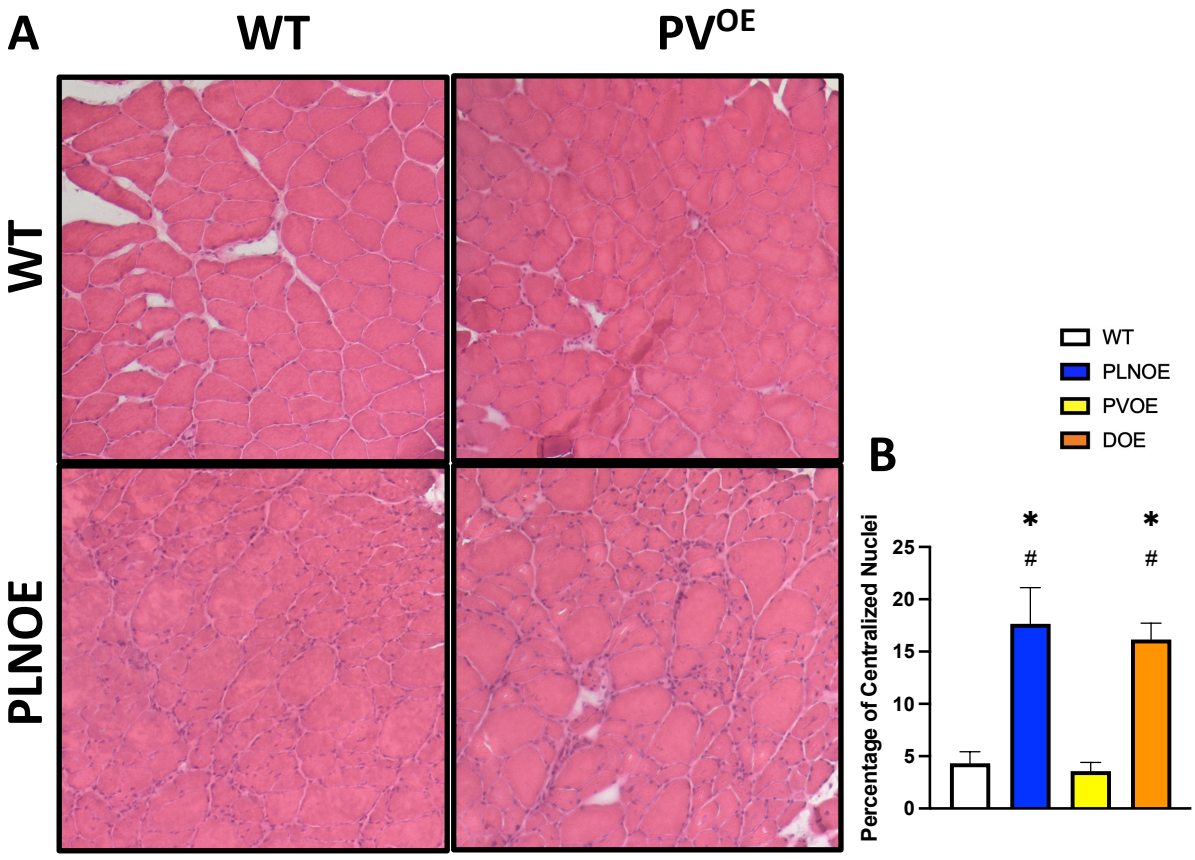

Figure 3: Parvalbumin overexpression did not improve the percentage of centralized nuclei in diseased soleus. (A) Representative images of H&E stain in WT (n=4), PLN^{OE} (n=4), PV^{OE} (n=5), and DB^{OE} (n=4). (B) Quantification of the proportion of centralized nuclei. * indicates a significant difference from WT ($p<0.05$) and # indicates a significant difference from PV^{OE} ($p<0.05$).

SDH stains were performed to visualize the oxidative activity in cross-sections of soleus muscles (Fig. 3B). Within PLN^{OE} tissue the presence of central aggregations were observed representing a centralization of oxidative activity. This feature was also observed with DB^{OE} tissue but appeared to be absent in WT and PV^{OE} tissue.

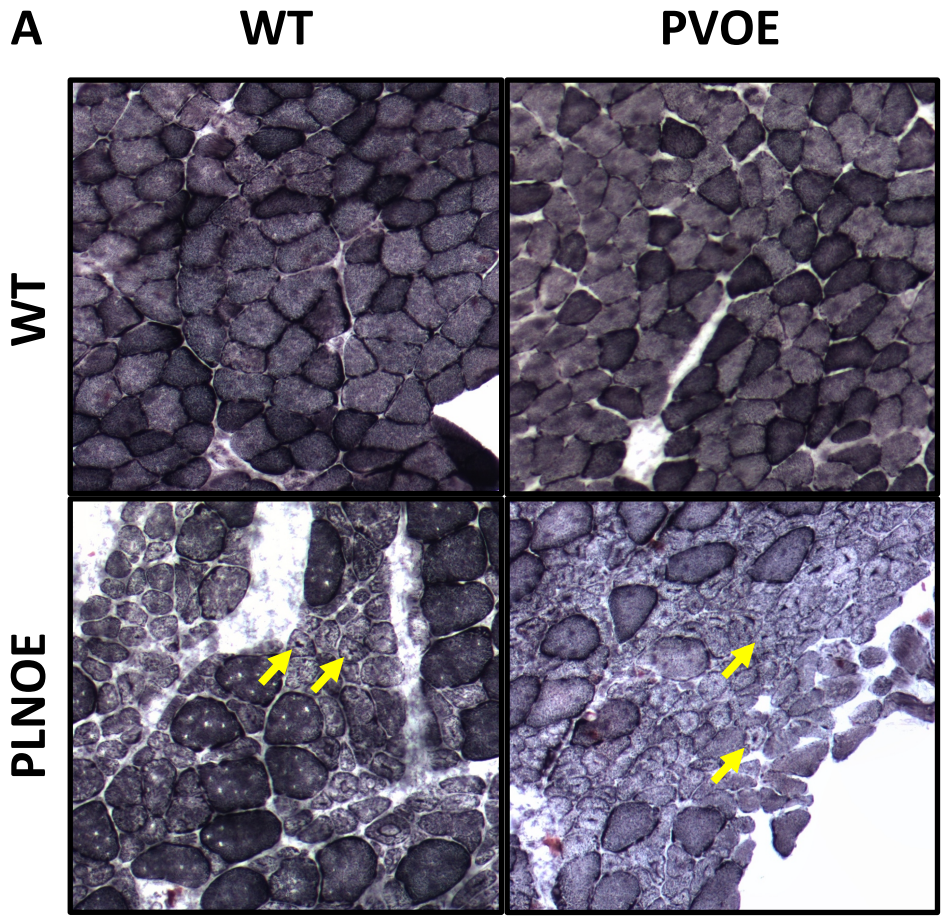

Figure 4: Central aggregations during SDH persist with parvalbumin overexpression (A) Representative images of SDH stain. Arrows point to fibers displaying central aggregations of

VanGeison stains were conducted to quantify collogen infiltration within muscle tissue. The quantification of collogen allowed for the comparison of fibrosis between groups. Statistical analysis revealed significantly greater amounts of fibrosis in the PLN^{OE} and DB^{OE} genotypes when compared to the WT ($p<0.05$, $p<0.05$, respectively) and PV^{OE} genotypes ($p<0.05$, $p<0.05$, respectively). However, there was no differences in fibrosis observed between the PLN^{OE} and DB^{OE} groups.

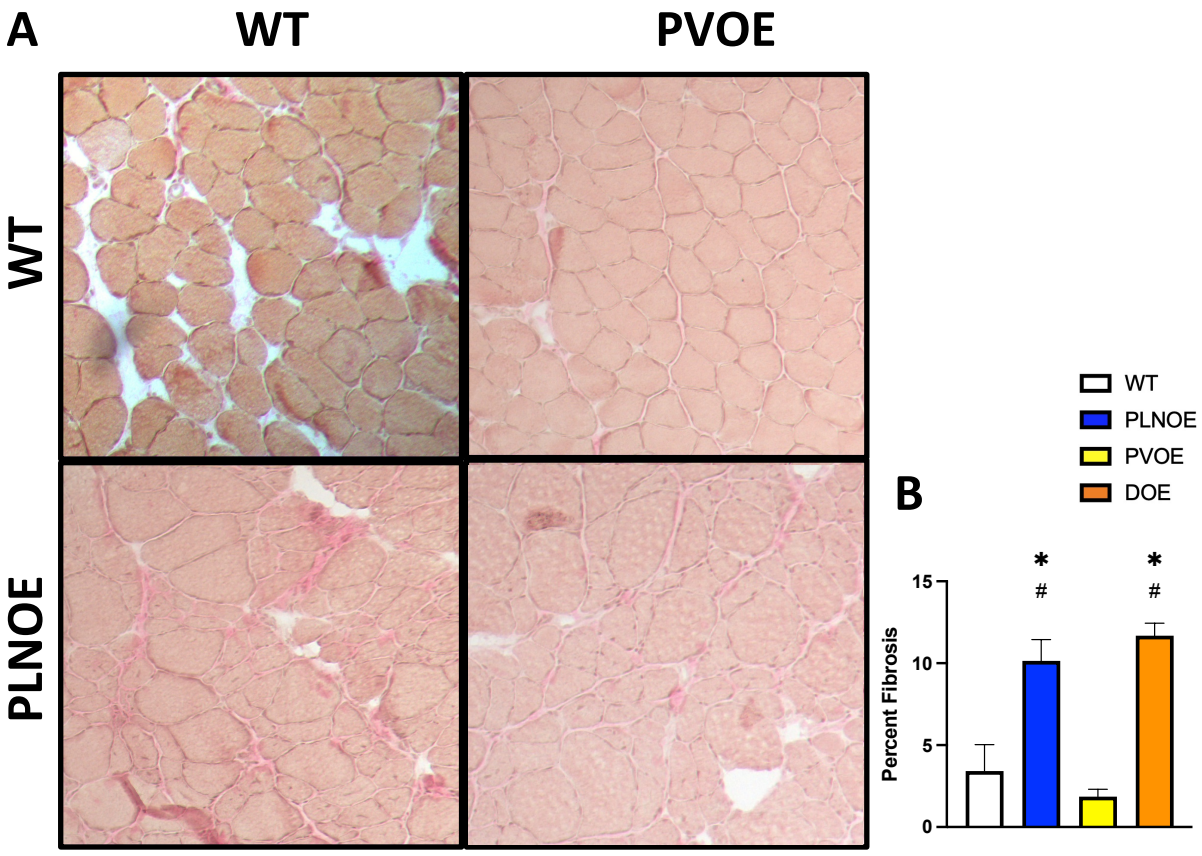

Figure 5: Parvalbumin overexpression did not improve fibrosis in diseased soleus. (A) Representative images of VanGeison stain in WT (n=4), PLN^{OE} (n=6), PV^{OE} (n=5), and DB^{OE} (n=6). (B) Quantification of the proportion of collogen infiltration. * indicates a significant difference from WT ($p<0.05$) and # indicates a significant difference from PV^{OE} ($p<0.05$).

Muscle Fibre Type and Cross-Sectional Area

Immunofluorescent staining (Fig. 6A) was conducted to quantify the changes in cross-sectional area and the distribution of fibre type in the collected soleus tissue. Analysis found that the CSA of type I fibres in the soleus muscle of diseased animals was smaller (Fig. 6B). Specifically, the CSA of type I fibres of PLN^{OE} and DB^{OE} mice were significantly reduced in comparison to WT ($p<0.05$, $p<0.05$, respectively). This trend was similar when comparing the diseased genotypes to PV^{OE} as the PLN^{OE} and DB^{OE} genotypes had a significantly lower CSA when compared to PV^{OE} ($p<0.05$, $p<0.05$ respectively). There were no differences found in the CSA of type I fibres between the PLN^{OE} and DB^{OE} groups ($p>0.05$) or between the WT and PV^{OE} groups ($p>0.05$). In contrast, CSA analysis of type IIA fibres found there was hypertrophy associated with the disease genotype (PLN^{OE} and DB^{OE}) (Fig. 6C). In comparison to WT, the PLN^{OE} ($p<0.05$) and DB^{OE} groups ($p<0.05$) had a significantly higher type IIA fibre CSA in soleus. Interestingly, no differences ($p>0.05$) in type IIA fibre CSA were found between PV^{OE}, PLN^{OE}, and DB^{OE} mice. Furthermore, no significant differences ($p>0.05$) were found in the CSA of Type IIX fibres between any of the groups (Fig. 6D).

With respect to muscle fibre type in soleus, the PLN^{OE} and DB^{OE} genotypes displayed a greater proportion of type I fibres in comparison to WT ($p<0.05$ and $p<0.05$, respectively) and PV^{OE} ($p<0.05$ and $p<0.05$, respectively) (Fig. 6E). No differences were found in the proportion of type I fibres between the PLN^{OE} and DB^{OE} group ($p>0.05$). Furthermore, the greater type I fibre percentage observed in PLN^{OE} and DB^{OE} was accompanied by a decreased percentage of type IIA fibres among the PLN^{OE} and DB^{OE} genotypes compared to WT ($p<0.05$ and $p<0.05$, respectively) and PV^{OE} ($p<0.05$ and $p<0.05$, respectively). Importantly, there was no difference in the percentage of type IIA fibres between PLN^{OE} and DB^{OE} mice ($p>0.05$). The percentages of

pure type IIX and hybrid type I/IIA and type IIA/IIX fibres were small and there were no differences ($p>0.05$) in these fibre type percentages between any of the groups (Fig. 6E).

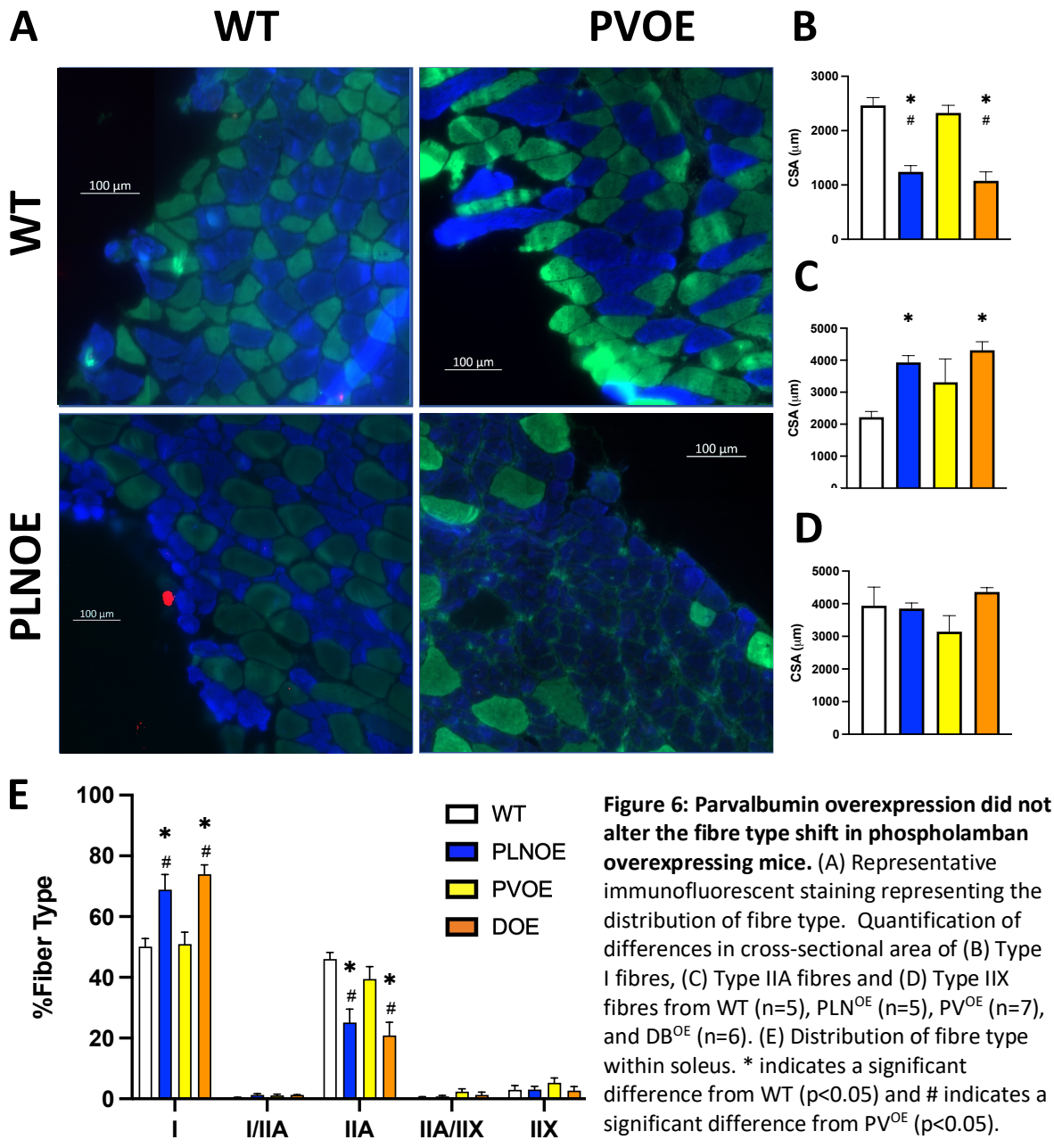

Figure 6: Parvalbumin overexpression did not alter the fibre type shift in phospholamban overexpressing mice. (A) Representative immunofluorescent staining representing the distribution of fibre type. Quantification of differences in cross-sectional area of (B) Type I fibres, (C) Type IIA fibres and (D) Type IIX fibres from WT (n=5), PLN^{OE} (n=5), PV^{OE} (n=7), and DB^{OE} (n=6). (E) Distribution of fibre type within soleus. * indicates a significant difference from WT ($p<0.05$) and # indicates a significant difference from PV^{OE} ($p<0.05$).

SERCA Function

A Ca^{2+} uptake assay was used to examine SERCA function in soleus homogenates. Ca^{2+} uptake was assessed at free Ca^{2+} concentrations of 1000 nM (Fig. 7A) and 500 nM (Fig. 7B). At a Ca^{2+} concentration of 1000 nM the rate of Ca^{2+} uptake among diseased genotypes, PLN^{OE} and DB^{OE}, was reduced in comparison to WT (WT vs PLNOE $p<0.05$, WT vs DB^{OE} $p<0.05$) and PV^{OE} (PV^{OE} vs PLN^{OE} $p<0.05$, PV^{OE} vs DB^{OE} $p<0.05$). A similar pattern was observed at a Ca^{2+} concentration of 500 nM where the rate of Ca^{2+} uptake was lower among diseased genotypes in comparison to the WT group (WT vs PLN^{OE} $p<0.05$, WT vs DB^{OE} $p<0.05$) and the PV^{OE} group (PV^{OE} vs PLN^{OE} $p<0.05$, PV^{OE} vs DB^{OE} $p<0.05$). There were no significant differences in the rate of Ca^{2+} uptake observed between the PLN^{OE} genotype and the DB^{OE} genotype at 1000 nM ($p>0.05$) and at 500 nM ($p>0.05$) or between the WT and PV^{OE} genotypes at 1000 nM ($p>0.05$) and at 500 nM ($p>0.05$). Additionally, starting [Ca^{2+}] was recorded as the Ca^{2+} concentration immediately following the addition ATP which initiated the uptake assay. No differences were observed in among all for groups. Specifically, there were no differences when comparing WT (PLN^{OE}; $p>0.05$, DB^{OE}; $p>0.05$) and PV^{OE} (PLN^{OE}; $p>0.05$, DB^{OE}; $p>0.05$) to diseased tissue. Furthermore, there were no differences observed when comparing WT versus PV^{OE} ($p=0.989$) and when comparing PLN^{OE} and DB^{OE} ($p>0.05$).

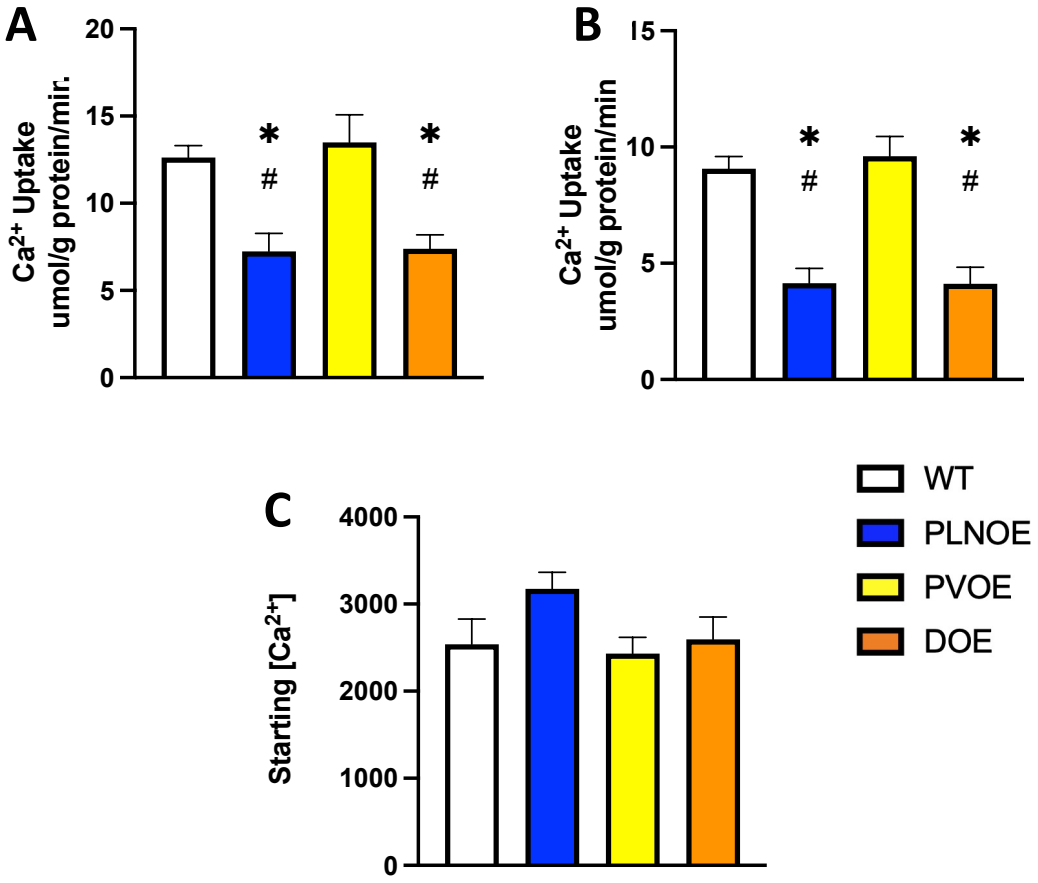

Figure 7: Parvalbumin overexpression does not alter the rate of Ca^{2+} uptake in soleus tissue. (A) Ca^{2+} uptake at 1000 nM $[Ca^{2+}]_f$ and (B) 500 nM $[Ca^{2+}]_f$ from WT (n=7), PLN^{OE} (n=7), PV^{OE} (n=7), and DB^{OE} (n=6). * indicates a significant difference from WT ($p<0.05$) and # indicates a significant difference from PV^{OE} ($p<0.05$). (C) Starting Ca^{2+} from the Uptake Assay recorded as the highest Ca^{2+} concentration documented on the uptake curve.

Calcium Handling Proteins

Western blotting was used to quantify proteins involved with Ca^{2+} sequestration. There were no differences ($p>0.05$) in SERCA1a expression in soleus among genotypes (Fig. 8A). Probing for SERCA2a in soleus revealed that PLN^{OE} and DB^{OE} genotypes had a significantly greater quantity in comparison to WT ($p<0.05$, $p<0.05$, respectively) and PV^{OE} ($p<0.05$, $p=$ $p<0.05$, respectively) (Fig. 8B). However, there were no differences ($p>0.05$) found in SERCA2a quantity between PLN^{OE} and DB^{OE} genotypes or between WT and PV^{OE} genotypes (Fig. 8B). Additionally, PLN and pPLN contents were quantified and converted into a ratio. As expected, probing for PLN revealed a greater amount present in PLN^{OE} and DB^{OE} tissue compared to WT ($p<0.05$, $p<0.05$, respectively), and PV^{OE} ($p<0.05$, $p<0.05$, respectively) (Fig. 8C). There were no differences in PLN content found between PLN^{OE} and DB^{OE} genotypes ($p>0.05$) or between WT and PV^{OE} genotypes ($p>0.05$) (Fig. 8C). This pattern of expression was also found with pPLN, as PLN^{OE} and DB^{OE} genotypes had a significantly greater quantity of pPLN in comparison to the WT ($p<0.05$, $p<0.05$, respectively) and PV^{OE} genotype ($p<0.05$, $p<0.05$, respectively) (Fig. 8D). There were no differences observed in pPLN expression between PLN^{OE} and DB^{OE} ($p>0.05$) or between WT and PV^{OE} ($p>0.05$) (Fig. 8D). Despite the group differences found in the expression of PLN and pPLN, there were no significant differences found in the pPLN/PLN ratio between genotypes, although there were trends towards a reduction in the pPLN/PLN in the PLN^{OE} ($p=0.09$) and DB^{OE} ($p=0.10$) groups compared to WT.

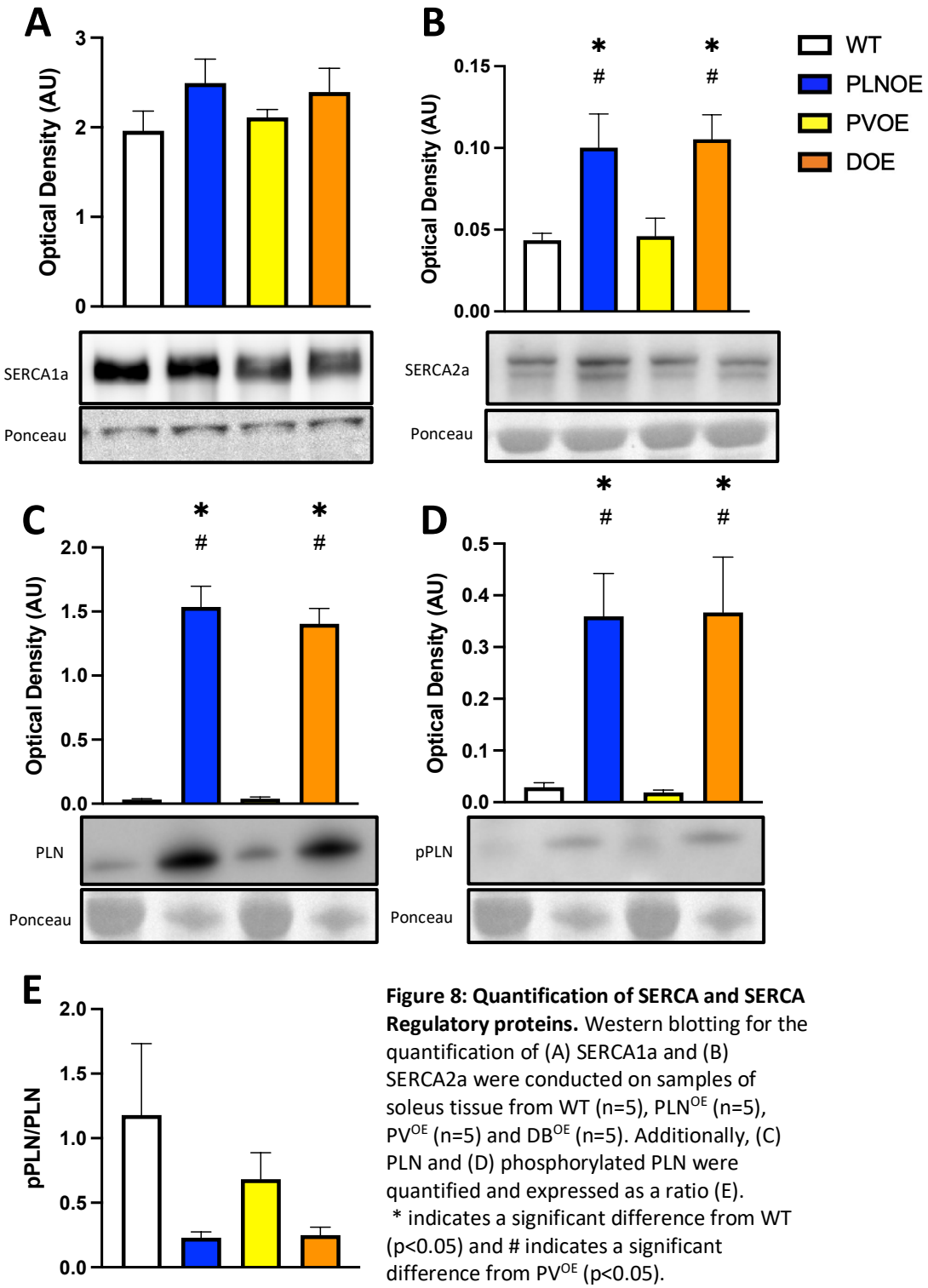

Figure 8: Quantification of SERCA and SERCA Regulatory proteins. Western blotting for the quantification of (A) SERCA1a and (B) SERCA2a were conducted on samples of soleus tissue from WT (n=5), PLN^{OE} (n=5), PV^{OE} (n=5) and DB^{OE} (n=5). Additionally, (C) PLN and (D) phosphorylated PLN were quantified and expressed as a ratio (E). * indicates a significant difference from WT ($p<0.05$) and # indicates a significant difference from PV^{OE} ($p<0.05$).

The expression of the Ca^{2+} buffering protein PV was subdivided into endogenous PV (Fig. 9A) and the overexpressed isoform; PVHA (Fig. 9B). While there were no differences ($p>0.05$) in endogenous PV expression found among genotypes, the PVHA expression was significantly higher in the PV overexpressing groups PV^{OE} and DB^{OE} when compared to the WT ($p<0.05$ vs PV^{OE} and $p<0.05$ vs DB^{OE}) and PLN^{OE} ($p<0.05$ vs PV^{OE} and $p<0.05$ vs DB^{OE}) groups. Endogenous PV and PVHA were also summed together to assess total PV (Fig. 9C). Total PV was significantly higher in the PV overexpressing groups in comparison to the WT ($p<0.05$ vs PV^{OE} and $p<0.05$ vs DB^{OE}) and PLN^{OE} ($p<0.05$ vs PV^{OE} and $p<0.05$ vs DB^{OE}) groups.

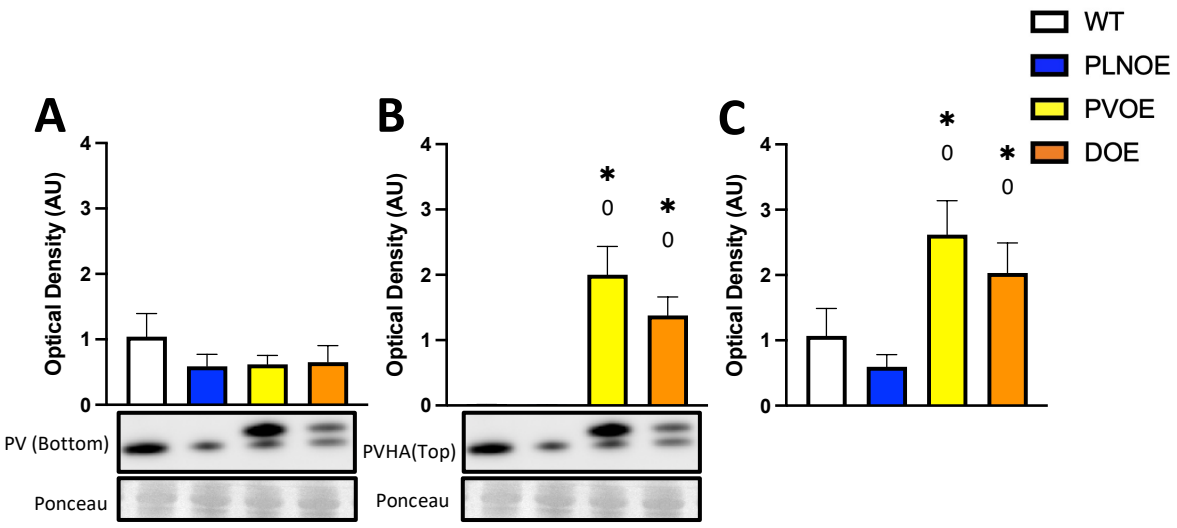

Figure 9: Quantification of Parvalbumin. Western blotting for the quantification of (A) endogenous PV and (B) PVHA were conducted on samples of soleus tissue from WT (n=5), PLN^{OE} (n=5), PV^{OE} (n=5) and DB^{OE} (n=5). Additionally, endogenous PV and the upregulated PVHA were summed to visualize total PV (C). * Indicates a significant difference from WT ($p<0.05$) and 0 indicates a significant difference from PLN^{OE} ($p<0.05$).

Calcineurin and NFAT

Western blotting was also used to assess if increased parvalbumin expression altered Ca^{2+} signalling. To assess Ca^{2+} signalling, calcineurin (Fig. 10A) and the ratio of phosphorylated NFAT (pNFAT) to total NFAT (Fig. 10B) were quantified. There were no significant differences ($p>0.05$) observed in either the ratio of pNFAT to total NFAT or in the content of calcineurin among genotypes.

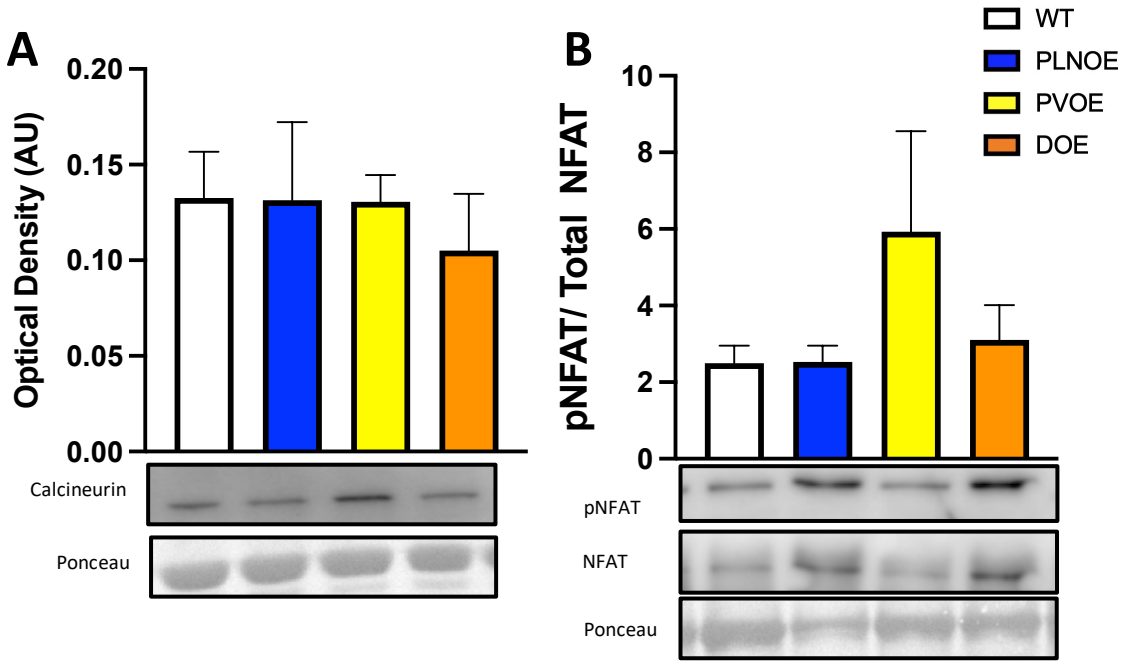

Figure 10: Quantification Proteins involved with Ca^{2+} signalling. Additionally, calcineurin was quantified on samples of soleus tissue from WT (n=6), PLN^{OE} (n=6), PV^{OE} (n=6) and DB^{OE} (n=6) (A). Western blotting for the quantification of pNFAT and total NFAT which were visualized in a ratio (B).

Discussion

The purpose of this project was to examine if overexpressing the Ca^{2+} buffering protein PV would attenuate the progression of CNM caused by PLN overexpression. PLN is a negative inhibitor of SERCA and consequently its overexpression causes impairments in Ca^{2+} sequestration leading to a myopathic phenotype. Logically, if elevated $[Ca^{2+}]_i$ is responsible for the pathogenesis of CNM, the introduction of a Ca^{2+} buffer may improve the rate of $[Ca^{2+}]_i$ decay and reduce $[Ca^{2+}]_i$, thus reducing the CNM phenotype. However, an examination of the data suggests that the increased expression of PV: (1) did not diminish the atrophy observed in the soleus of PLN^{OE} mice, (2) did not improve the histological markers of the PLN^{OE} disease phenotype, (3) did not improve the contractile function or the Ca^{2+} uptake of the affected muscle, and (4) did not attenuate the fibre type shift increasing the proportion of type I fibres. In this myopathic model, overexpressing PV does not appear to be a feasible treatment for attenuating disease progression.

For this project, soleus tissue was used because it was the only muscle which previous research had detected both signs of myopathy from PLN overexpression and expression of the PVHA transgene (Chin et al., 2003; Fajardo et al., 2015, 2016, 2017). Soleus muscles were analyzed both in absolute weight and as a ratio normalized to body weight. Both measurements were reported because past research with PLN^{OE} mice has not involved measures of body composition. This PLN^{OE} myopathy manifests in greater severity in postural muscles which could affect activity levels (Fajardo et al., 2015). Fajardo et al has found a trending reduction in total activity in PLN^{OE} mice compared to WT mice (Fajardo et al., 2017). Changes in activity could alter body composition which could potentially skew soleus weights when normalized to

body weight. Both absolute and normalized analyses revealed a significant decrease in muscle weight in the animals expressing the PLN^{OE} transgene. This study found PLN^{OE} mice had a 29% reduction in absolute soleus weight and 24% reduction in soleus weight normalized to BW when compared to the WT controls. These findings align with previous studies which have also reported reductions in soleus weights within PLN^{OE} mice and rabbits (Fajardo et al., 2015; Song et al., 2004). Specifically within PLN^{OE} mice, Fajardo et al found a 43% reduction in PLN^{OE} absolute soleus weight compared to WT (Fajardo et al., 2015). Furthermore, this study also reproduced findings from Chin et al in that there were no differences in soleus weight observed between the PV^{OE} and WT (Chin et al., 2003). Of primary interest, there were no differences in absolute and normalized soleus weight between the PLN^{OE} and DB^{OE} groups indicating that the overexpression of PV did not attenuate muscle atrophy in this disease model.

A histological analysis of centralized nuclei and fibrosis were used to quantify the amount of degenerative/regenerative cycling found in this model of CNM. In myopathic models with repeated injuries, nuclei are often positioned in the center of the myocyte as transcriptional activity is upregulated to repair damaged tissue (Folker & Baylies, 2013). Furthermore, fibrosis is also commonly detected in skeletal muscle myopathies with repeated injuries as a result of the maladaptive infiltration of fibroblasts and extracellular matrix into the endomysium (Mann et al., 2011). A potential explanation for the increase in fibrosis in this PLN^{OE} model may be due to excess Ca^{2+} increasing calpain and caspase activity. Previous work by Fajardo and colleagues have detected elevated calpain and caspase activity in PLN^{OE} mice (Fajardo et al., 2017). Increases in protease activity could result in this cycling of degenerative and regenerative pathways which could also eventually lead to the observed muscle atrophy. The findings in this project align with previous research which found soleus muscle from PLN^{OE} mice contained a

greater proportion of centralized nuclei and fibrosis compared to their WT counterparts (Fajardo et al., 2015, 2017). This phenotype has also been observed in the *mdx* mouse model for Duchene's Muscular Dystrophy (DMD) (Carnwath & Shotton, 1987; McDonald et al., 2015). There are differences however between these disease models. In *mdx* mice, contractions cause disruptions in the myocyte plasma membrane due to the structural instability of myofibres (Hopf et al., 2007). In contrast, the pathogenesis of PLN^{OE} related CNM occurs through the inhibition of SERCA resulting in abnormal Ca^{2+} handling. However, research in both myopathy models have indicated that $[Ca^{2+}]_i$ is elevated and results in increased protease activity (Alderton & Steinhardt, 2000; Fajardo et al., 2017; Hopf et al., 2007; Whitehead et al., 2006). Interestingly, DMD research has found that improving Ca^{2+} uptake can reduce centrally located nuclei and fibrosis. In *mdx* mice, SERCA1 overexpression ameliorated the central nuclei phenotype in soleus tissue (Goonasekera et al., 2011). In that same study it was found that lowering $[Ca^{2+}]_i$ allowed fibrosis within *mdx* soleus to remain near WT levels (Goonasekera et al., 2011). The increased SERCA1 expression was associated with reductions in the time of Ca^{2+} decay and a reduction in resting $[Ca^{2+}]_i$ which appeared to improve the pathology (Goonasekera et al., 2011). As a Ca^{2+} buffer, PV should also act to sequester $[Ca^{2+}]_i$, however its overexpression did not improve the percentage of centralized nuclei or fibrosis in the DB^{OE} mice when compared to the PLN^{OE} mice. A possible explanation could be that the PV buffering capacity is not strong enough to counteract the increase in $[Ca^{2+}]_i$ brought on by PLN overexpression. Although PV may be buffering $[Ca^{2+}]_i$, it may not be lowering $[Ca^{2+}]_i$ enough to prevent it from interacting with the Ca^{2+}-sensing proteins of degradation pathways. Consequently, the percentage of centralized nuclei may remain unchanged in the DB^{OE} mice because the overexpressed PV is not decreasing the degenerative/regenerative cycling.

Coupled with the centrally located nuclei, SDH staining revealed central aggregations of oxidative activity in atrophied fibres. These aggregations support previous research reporting a centralization of oxidative activity observed in type I fibres of mice overexpressing PLN (Fajardo et al., 2015, 2017). A possible explanation for the abnormal distribution of oxidative activity may lie in other genetic models of CNM. Other models of CNM have been attributed to mutations in membrane trafficking proteins including Dynamin-2 and Myotubularin (Jungbluth & Gautel, 2014). Although PLN is not directly involved with membrane trafficking, Fajardo and colleagues have reported a 5-fold increase in the expression of dynamin 2 in PLN^{OE} mice (Fajardo et al., 2015). These findings suggest that impaired Ca^{2+} sequestration may disrupt membrane handling which could explain central aggregations of oxidative activity. In this project, SDH stains of DB^{OE} mice continued to present central aggregations like those observed in the PLN^{OE} group suggesting the intervention of overexpressed PV did not affect the pathological centralization of the mitochondria. Dynamin 2 was not assessed in this thesis however, the results suggest PV overexpression likely did not affect dynamin 2 expression in this model.

Although this histological analysis was used to compare the disease progression between groups, contradictory evidence suggests it may not always be the best indicator of disease severity. Past research by Chambers et al, who used a cyclosporin A treatment in PLN^{OE} mice, found improvements in soleus contractility, but that did not translate into improvements in histological measurements (Chambers, unpublished). However, other work from the Tupling lab has shown that alleviating PLN inhibition on SERCA in PLN^{OE} mice with formoterol treatment can reduce fibrosis and centralized nuclei (Reitze, unpublished). Together, this research suggests that histological analyses in CNM mice may not always indicate disease severity. Thus,

histological staining should be coupled with functional analyses to properly understand disease progression.

Functional contractile measures of intact soleus muscles were used to quantify inotropic and lusitropic properties of the collected tissue. An analysis of force production normalized to soleus weight revealed no significant differences among the groups. However, the graphical visualization of the data illustrates a trend in which the PLN^{OE} and DB^{OE} groups are depressed in force production when compared to WT and PV^{OE} mice. This visual trend occurred at frequencies greater than 50 Hz. The statistical insignificance observed among force production data may be due to a large degree of variance and low sample size. Like the observed trend, previous work has found that PLN^{OE} mice do have a reduced normalized force production occurring at stimulation frequencies of 100 Hz (Fajardo et al., 2017). This may be explained by the greater amount of fibrosis found in diseased tissue. With greater fibrosis, a smaller proportion of the soleus cross-sectional area can form crossbridges resulting in a smaller fraction of the muscle contributing to force production. Furthermore, in reference to the PV^{OE} genotype, previous research has shown an 8% and 14% reduction in force at 30 and 50Hz, respectively (Chin et al., 2003). Although not significant, data from this project revealed a comparable reduction of 17%, 16%, 11%, and 5% in the mean force production at 20, 30, 40 and 50Hz, respectively. The reduction of force in PV^{OE} mice may be explained by PV buffering $[Ca^{2+}]_i$ resulting in less TnC saturation (Westerblad & Allen, 1993). Importantly, there were no differences statistically and visually between the force frequency curves of the DB^{OE} group and the PLN^{OE} group. The similarity in force production among these two groups can have both positive and negative interpretations. Firstly, the DB^{OE} force production is not reduced when compared with PLN^{OE} mice like it has been shown to be in PV^{OE} versus WT mice. This may

suggest that PV buffering is not reducing TnC saturation. As a slow calcium buffer, PV is dependent on Mg^{2+} becoming unbound from the calcium binding site before beginning to buffer calcium (Hou et al., 1991; Schwaller et al., 1999). If SERCA inhibition is resulting in elevated $[Ca^{2+}]_i$, then $[Ca^{2+}]_i$ may rise well above concentrations needed for TnC saturation before PV can begin buffering. When PV begins buffering $[Ca^{2+}]_i$, the buffering capacity of PV may not lower $[Ca^{2+}]_i$ below TnC saturating levels. As a result, force production is preserved in the DB^{OE} group. However, since there were no improvements in force production among the DB^{OE} group versus the PLN^{OE} group this would suggest that the PV overexpression is not improving the disease associated weakness. In this regard, PV does not appear to be worsening or improving force production.

Force development kinetics, including rates of force production (+dF/dt) and time to peak tension were also analyzed. No differences were found in +dF/dt among the four groups across all frequencies. In this analysis there appeared to be a high degree of variability among samples. However, the findings that +dF/dt is not significantly different is unexpected for two reasons. Firstly, with the presence of myopathy, there would be expected functional differences due to reductions in crossbridge formation. With a decrease in crossbridge formation, less force would be able to be generated per unit of time. Additionally, in this disease model there is a fibre type shift toward type I fibres. Characteristically, type I fibres have a slower contractile speed due to the rate of ATP hydrolysis by the myosin heavy chain ATPase (Taylor. et al., 1974). Thus, it would be expected that a shift toward more type I fibres results in slower rates of contraction. Furthermore, there appears to be no differences in time to peak tension among the groups at both twitch and 100 Hz. In contrast to these findings, Fajardo et al found a significant reduction in single twitch +dF/dt in PLN^{OE} mice versus WT (Fajardo et al., 2017). These findings would

suggest that the diseased mice assessed in this thesis do not have impairments in SR Ca^{2+} loading and Ca^{2+} release from the SR. The differences observed in rate of contraction in this thesis versus previous research may be due to low sample size and high variability. Another contributor to these contrasting findings may be from the strain differences as mice used in this project were on a mixed FBV/N / CD1 background while Fajardo et al used FBV/N mice (Fajardo et al., 2017).

In compliment to contractile rate, the rate of relaxation was also quantified. At twitch, there appeared to be no differences in the rate of relaxation among all four genotypes. However, as frequency increased a visual trend became apparent in which the WT and PV^{OE} groups appeared to have faster rates of relaxation in comparison to the PLN^{OE} and DB^{OE} groups. However due to the sizeable variability between samples, the only data yielding statistical significance was a slower -dF/dt in the DB^{OE} group versus the WT group at 40 Hz. Interestingly, PV overexpression did not appear to influence the rate of relaxation in the healthy groups; WT vs PV^{OE} and the diseased groups; PLN^{OE} vs DB^{OE}. The diseased phenotype brought on by PLN overexpression resulted in slower rates of relaxation. Within the DB^{OE} mice, PV overexpression occurs in the type I fibres, and there was a shift toward a greater distribution of type I fibres in the disease phenotype. As illustrated by the western data, PVHA and total PV were significantly higher in DB^{OE} versus PLN^{OE} mice. Despite this difference in PV expression, it did not improve the rate of relaxation in the DB^{OE} group. Innately, PV is found in fast twitch fibres however in this model the PVHA transgene is overexpressed in slower fibres. It is possible that the PV-Ca^{2+} binding dynamics (such as the on/off binding rates) have been evolutionarily fine tuned for the contractile properties of type II fibres. As a result, the buffering capabilities of PV may not function as effectively in fibres where prolonged contractions can be sustained. With sustained contractions, the PV Ca^{2+} binding site may become saturated before neural signalling ceases and

relaxation occurs. As a result, PV will not be contributing to $[Ca^{2+}]_i$ sequestration during relaxation. This reasoning may also explain why there were no differences in half relaxation time between DB^{OE} and PLN^{OE} groups at 100Hz. Furthermore, during twitch there were also no significant differences among the DB^{OE} and PLN^{OE} groups. At twitch, it is possible that PV would not have a role in relaxation due to the above-mentioned time delay at which Mg^{2+} must vacate the Ca^{2+} binding site. Some studies have stated that the off rate of Mg^{2+} can range from 3 to 25 seconds (Hou et al., 1991; Lee et al., 2000). In contrast, the duration of a normal muscle twitch is typically no more than 100 ms (Heskamp et al., 2021). In our results there were no significant differences between diseased groups and healthy groups for half relaxation time at twitch and 100 Hz. However there did appear to be increased time in the means of groups overexpressing PLN. It is possible that the variability in our data made it difficult to detect differences among groups. Past research has found the PLN overexpression reduces both SERCA activity and the maximal rate of Ca^{2+} pumping. Thus, the trending reduction of -dF/dt in diseased tissue is likely due to the inhibitory effect overexpressed PLN is having on SERCA function. This is supported by the results of the Ca^{2+} uptake assay.

The Ca^{2+} uptake assay is used to measure the rate of calcium sequestration in homogenized muscle samples. The Ca^{2+} uptake assay revealed significant reductions in the DB^{OE} and PLN^{OE} groups compared to the WT and PV^{OE} groups at $[Ca^{2+}]$ of 1000 nM and 500 nM. This aligns with our current understanding of PLN as a SERCA inhibitor, with greater PLN expression there would be an expected greater inhibition of SERCA. Previous work by Fajardo and colleagues have found similar findings in that PLN^{OE} mice had reduced Ca^{2+} uptake (Fajardo et al., 2015). Furthermore, that study also showed a reduction in Ca^{2+} affinity and reduction in V_{max} in PLN^{OE} mice vs WT mice further supporting the theory that PLN overexpression is

resulting in attenuated Ca^{2+} uptake. In this experiment, there were no differences among the PLN^{OE} and DB^{OE} groups. Although this project is focused on the effect PV had in Ca^{2+} sequestration, it is likely this assay only detected the contributions of Ca^{2+} sequestration by SERCA. In the Ca^{2+} assay protocol all ingredients, including Ca^{2+} and homogenized sample, were added to the working solution before the assay began. The assay would then commence with the addition of ATP to the working solution to initiate Ca^{2+} pumping by SERCA. By the time ATP was added, the PV situated outside of reformed plasma membrane vesicles would have likely already buffered cytosolic Ca^{2+}. As a result, PV overexpression may not have contributed to the rate of Ca^{2+} uptake. To determine if PV was affecting Ca^{2+} sequestration prior to the addition on ATP, starting [Ca^{2+}] was analyzed. No differences in starting [Ca^{2+}] were found among the four genotypes. The uniformity in starting [Ca^{2+}] among the groups could be because PV is present in all groups. The PVHA transgene upregulates PV in type I fibres, however the innate PV would still be present in type II fibres. As shown in the PV western blotting, endogenous PV was still expressed in all four groups, and the PVHA transgene was specific to the PV^{OE} and DB^{OE} groups. Unfortunately, this assay is limited to whole muscle homogenates which makes it difficult to determine the effect PV is having in the type I fibres. Additionally, due to the unstructured nature of homogenized tissue there was likely other buffering proteins present, namely calsequestrin (CSQ). CSQ typically exists exclusively in the SR however in homogenized tissue, the disruption in membranes may result in CSQ existing within the homogenate outside of reformed vesicles. If CSQ is present in the homogenate of all groups, it could have partially masked any effects the PV overexpression may have had.

Another factor that could have affected the rate of Ca^{2+} uptake in this assay is the phosphorylation status of PLN. Phosphorylation of PLN can be influenced by $[Ca^{2+}]_i$. When

$[Ca^{2+}]_i$ is elevated this will activate CAMKII which can phosphorylate PLN and reduce its inhibitory effect on SERCA. In a scenario where PV is introduced, it is possible that any PV buffering could result in less PLN phosphorylation and consequentially greater SERCA inhibition. If this were to occur, any Ca^{2+} buffering by PV may be offset by the reduced PLN phosphorylation. Taking this into consideration, the expression of phosphorylated PLN (p-PLN) and PLN were quantified through western blotting. Both PLN and p-PLN were significantly greater in quantity among PLN overexpressing groups; PLN^{OE} and DB^{OE}, when compared to WT and PV^{OE}. This aligns with previous research where the PLN overexpressing genotype results in a greater amount of both PLN and p-PLN. Previous reports have also shown that the ratio of p-PLN/PLN was reduced in diseased tissue suggesting the equilibrium in PLN phosphorylation had shifted toward more unphosphorylated PLN (Fajardo et al., 2017). Similarly, this thesis found a trend toward significance when comparing the PLN^{OE} ($p=0.09$) group and the DB^{OE} ($p=0.10$) group to WT. However, there were no differences found in the pPLN/PLN ratio between the PLN^{OE} and DB^{OE} groups suggesting PV overexpression in not altering the phosphorylation status of PLN.

Another consideration for the decreased Ca^{2+} uptake among diseased muscle is the associated fibre type shift. Traditionally type II fibres relax faster than type I fibres due to the greater quantity of SERCA expressed within the SR membrane (Fajardo et al., 2013). With a shift toward a higher proportion of type I fibres, SERCA quantity could change thus affecting Ca^{2+} uptake. To assess the effect the fibre type shift had on SERCA expression, SERCA1a and SERCA2a were quantified. No differences were found in the expression of SERCA1a among all four groups. SERCA1a is expressed in both fibre types which can explain why a shift in fibre type does not appear to be causing change in SERCA1a expression. Differences in SERCA2a

expression were detected in PLN^{OE} and DB^{OE} mice, which showed a significantly greater quantity of SERCA2a versus WT and PV^{OE}. These differences can likely be explained by a fibre type shift since SERCA2a is most highly expressed in the type I fibres. Interpreting the SERCA western blots together, it becomes apparent that SERCA expression is greater in soleus tissue overexpressing PLN. This would suggest that the impairments observed in the Ca^{2+} uptake are likely attributable to SERCA inhibition rather than changes in SERCA expression.

Logically, it would expected that SERCA inhibition would be greater in tissue overexpression PLN, as it is a natural SERCA inhibitory protein. However, the reduced Ca^{2+} uptake may also be partially derived from elevated ROS/RNS. Past research has shown SERCA is sensitive to oxidative stress resulting its inactivation (Dremina et al., 2007). Previously, Fajardo and colleagues have reported increased oxidative stress and increased protein nitrosylation in PLN^{OE} mice (Fajardo et al., 2015). Taken together, the impaired Ca^{2+} uptake from the PLN^{OE} and DB^{OE} mice in this thesis are likely in part due to SERCA inactivation from oxidative stress. Additionally, the lack of differences in Ca^{2+} uptake between the PLN^{OE} and DB^{OE} group may suggest that PV Ca^{2+} buffering reducing oxidative stress in the diseased muscle.

Immunohistochemistry was conducted to assess the proportion and cross-sectional area of fibre types. A common marker of CNM is specific hypotrophy of type I fibres (Romero & Bitoun, 2011). Specifically, in this study it was found that there was a significant reduction of cross-sectional area among the type I fibres of PLN^{OE} and DB^{OE} mice when compared to the WT and PV^{OE} groups. Furthermore, there is a significant increase in the cross-sectional area of type II fibres in the PLN^{OE} and DB^{OE} groups in comparison to the WT group. The change in fibre type distribution and cross-sectional area has been previously theorized to be part of a

compensatory response to maintain muscle function. In this disease model, type I fibres are most affected due to the overexpression of PLN embedded in the MHCI promoter. As a result, introducing this PLN overexpression reduces SERCA activity which can result in an increase in protease activity in the type I fibres. Increased protease activity subsequently results in atrophy of the affected fibre and by doing so would reduce the force producing capabilities in these fibres. By reducing the functionality of type I fibres, type II fibres become overloaded. This overloading of the type II fibres may explain the increase in cross sectional area through the upregulation of hypertrophic pathways. Furthermore, the overload stimuli may also be increasing Ca^{2+} signaling in the type II fibres, increasing CnA activity and promoting a shift toward type I fibres(Musarò et al., 1999; Parsons et al., 2004).

Previous reports have observed a shift toward a greater distribution of type I fibres in this disease model (Fajardo et al., 2015, 2017; Romero & Bitoun, 2011). Similar observations were made in this study with both the PLN^{OE} and DB^{OE} mice having a greater proportion of type I fibres and an accompanied reduction in type II fibres compared to the WT and PV^{OE} groups. Despite the observed fibre type shift, there were no differences found in the CnA content and the proportion of pNFAT and NFAT between all four groups. Previous research in PLN^{OE} mice has found a depressed ratio of pNFAT/NFAT when compared to WT controls. The depressed pNFAT/NFAT ratio shown in previous work is likely a result of two different factors. Firstly, in diseased fibres PLN inhibition results in elevated $[Ca^{2+}]_i$ which would likely increase the phosphatase activity of CnA thus reducing the proportion of pNFAT. Secondly, if the affected type I fibres have a reduced force output, this may result in the type II fibres experiencing greater loading. The compensatory overloading of the type II fibres may result in a prolonged elevation in $[Ca^{2+}]_i$. Consequently, CnA activity may increase causing these fibres to transition to type I.

When quantifying these proteins, the effect of these two pathways summate in depressing the ratio of pNFAT/NFAT. Despite this rational for the shift in pNFAT/NFAT, no differences were revealed between the four groups in this study. This project quantified the expression of NFATc1 as it is believed to be the isoform with the strongest association with MHCI expression (Ehlers et al., 2014). However, other research has suggested there may be redundancy among the Ca^{2+} dependent isoforms of NFAT. Indeed, past research by Calabria and colleagues has shown that NFATc1-4 all work cooperatively in controlling the expression of MHCI (Calabria et al., 2009). Other research has also shown there is a similarity in genomic binding domains of NFAT which has been shown to have redundancies in the pathways different isoforms effect (Crabtree & Olson, 2002; Ho et al., 1995). Although there may not be differences in NFATc1, other NFAT isoforms may have an altered phosphorylated to unphosphorylated ratio which could be leading to this fibre type shift. Furthermore, previous work which described the depressed pNFAT/NFAT ratio in PLN^{OE} mice was conducted in C57BL/6J mice which differs from this study which conducted analysis on animals with a mixed CD1 and FVB/n background. Other work conducted in PLN^{OE} mice on an FVB/n background has looked at NFAT expression and has also observed unexpected findings. In that study, PLN^{OE} mice treated with a CnA inhibitor displayed a depressed pNFAT/NFAT ratio compared to vehicle treated controls (Chambers, unpublished). The results from Chambers et al along with the findings from this thesis may suggest that quantifying NFATc1 alone may not be fully encompassing fibre type signalling.

Although PV did not improve the progression of CNM, other research has found transgenic PV to lessen disease progression in the heart (Wang et al., 2013). From this research it appears the function of the affected tissue is an important consideration when contemplating a transgenic PV intervention. As a postural muscle, soleus tissue can be subject to long periods of

sustained contraction. Sustained contractions may be problematic for a PV intervention if the length of contraction results in PV becoming saturated prior to the decay phase of EC coupling. In contrast, the heart is involuntary and maintains predictable patterns of contraction. The brief contractile patterns native to cardiac tissue may allow PV to contribute to the decay of Ca^{2+} transients more readily. Furthermore, the PV intervention which improved the cardiomyopathic model also underwent substantial analysis before the transgene was utilized in vivo (Wang et al., 2013). Indeed, researchers used computer modelling to alter the amino acid sequence within the PV-Ca^{2+} binding site to manipulate the affinity and on/off rate of Ca^{2+}. In doing this, these researchers were able to optimize the Ca^{2+} handling dynamics of PV so it would align with the predictable cardiac contractile pattern. For this project, no prior alterations were made to the transgenic PV sequence prior to its inception in vivo. Future research looking to utilize a PV intervention should consider the use of computer modeling first as it may yield greater specificity in meeting the needs of the focused tissue.

Future directions and Conclusion

This study attempted to improve the CNM phenotype brought on by PLN overexpression by overexpressing the cytosolic Ca^{2+} buffer PV. Evidence presented in this study suggests PV did not change the disease progression of CNM. The increased expression of PV did not attenuate the presence of fibrosis, reduce the increased percentage of centralized nuclei, diminish central aggregations of oxidative activity, or decrease the greater proportion of type I fibres. Additionally, PV did not improve any functional contractility measures or SERCA Ca^{2+} uptake function. Although PV did not improve the severity of CNM, there continues to be many avenues to further the understanding of CNM both in the PLN^{OE} mouse model and other genotypic models.

To progress the understanding of Ca^{2+} in CNM, future studies should include measures of $[Ca^{2+}]_i$. Early CNM literature has shown that Ca^{2+} dysregulation is present across several different models of this myopathy (Jungbluth & Gautel, 2014; Kramerova et al., 2008). Current research by Fajardo et al used PLN^{OE} mice to provide direct evidence for the role of Ca^{2+} dysregulation in CNM pathogenesis (Fajardo et al., 2015, 2017). Collectively this research has indirectly detected elevated $[Ca^{2+}]_i$ in CNM. This thesis attempted to counteract the elevated $[Ca^{2+}]_i$ in CNM through introducing a cytosolic Ca^{2+} buffer. However, a critical limitation in this study was that $[Ca^{2+}]_i$ was not directly evaluated. Without a direct measure of $[Ca^{2+}]_i$ it is difficult to determine the amount of buffering occurring in the cytosol. Quantifying $[Ca^{2+}]_i$ would offer more information on the magnitude and the rate at which $[Ca^{2+}]_i$ is buffered. Considering that the upregulated PV did not improve the CNM severity, measuring $[Ca^{2+}]_i$ transients within intact muscle may provide an explanation. Previous research in the Tupling lab has quantified $[Ca^{2+}]_i$ during EC coupling. However, this research was restricted to mouse lumbricals because a

small muscle size was necessary for the diffusion of Ca^{2+} -binding fluorescent dyes (Smith, 2014). This analysis could not be conducted in DB^{OE} mice as the intact soleus muscles collected in this study were too big for $[Ca^{2+}]_i$ analysis. As previously stated, the soleus was the only tissue that could be used for this thesis as it was the only muscle that developed the PLN^{OE} disease phenotype and expressed the PV overexpressing transgene. Encouragingly, Collet et al have had success in isolating individual fibres from mouse skeletal muscle and directly measuring $[Ca^{2+}]_i$ (Collet et al., 1999). These findings suggest that measuring $[Ca^{2+}]_i$ may be possible in PLN^{OE} mice. However, this proposed analysis must be coupled with fibre type identification because the PLN and PV overexpressing transgenes are specific to type I fibres. Measuring $[Ca^{2+}]_i$ in PLN^{OE} and DB^{OE} mice would provide greater insight on Ca^{2+} transients in the disease and how PV- Ca^{2+} interactions affect these Ca^{2+} transients.

To further understand the contribution of Ca^{2+} to the progression on CNM, a greater emphasis on mitochondrial measures should be considered. Previous reports of CNM have observed central aggregations of oxidative activity representing changes in the distribution of the mitochondria. Furthermore, research involving other genetic models of CNM have shown deficits in mitochondrial function (Hnia et al., 2011; Tinelli et al., 2013). Despite these findings, the role of the mitochondria in the pathogenesis and progression of CNM is yet to be fully explored. Previous research has shown that the mitochondria do uptake Ca^{2+} as a part of its normal function (Rizzuto et al., 1992; J. Zhou et al., 2011). During times of Ca^{2+} dysregulation, the mitochondria can uptake larger quantities of Ca^{2+} resulting in mitochondria swelling (Lemasters et al., 2009). If excessive Ca^{2+} uptake affects normal mitochondrial function, this could alter cellular metabolism and signaling pathways which work through the mitochondria. The mitochondria is a major site for ATP production, however the efficiency of oxidative

phosphorylation in PLN^{OE} mice is yet to be analyzed. Additionally, PV expression has also been shown to affect normal mitochondrial function as research by Lichvarova et al reported that introducing PV into canine kidney cells reduced mitochondrial volume and quantity (Lichvarova et al., 2018). Furthermore, research in mouse soleus has shown that PV overexpression decreases SDH activity (Chin et al., 2003). This compliments other research in PV knock out mice which reported increases in mitochondrial volume (G. Chen et al., 2001). To understand the effect of these transgenes, a quantification of mitochondrial metabolism should be considered. Furthermore, the involvement of the mitochondria in autophagic signaling cannot be overlooked. Past work by Fajardo et al analyzed autophagosome formation through quantifying LC3-I and LC3-II. Fajardo et al reported an increased ratio of LC3-II/LC3-I in PLN^{OE} versus WT mice suggesting greater autophagic signaling. Other pathways have been highlighted by Butera et al who have also shown evidence for hypertrophy signaling through mitochondrial Ca^{2+} uptake (Butera et al., 2021). Butera et al found a trophic effect in PV knockout tissue which became mitigated with the silencing of the mitochondrial Ca^{2+} uniporter (MCU) (Butera et al., 2021). Together this research indicates that although Ca^{2+} overload can be detrimental to mitochondrial function, there appears to be an essential minimal amount of Ca^{2+} influx into the mitochondria to maintain homeostasis. Future analyses in PLN^{OE} mice could involve reducing the expression of the MCU. If the elevated $[Ca^{2+}]_i$ in PLN^{OE} mice reduces the viability of the mitochondria, reducing Ca^{2+} import through MCU silencing could prevent the mitochondrial Ca^{2+} overload. The inclusion of analyses for mitochondrial Ca^{2+} handling in PLN^{OE} mice may provide a better understanding of the disease pathogenesis and progression.

Finally, within the current literature there remains ambiguity in the pathogenesis of CNM. Some research papers have reported its pathogenesis stems from mutations in Ca^{2+}

handling proteins, whereas other reports have suggested that CNM arises from dysfunctional membrane transport. A potential explanation could be that these two pathogenic mechanisms eventually affect a similar pathway. An example of this may involve the mitochondria where membrane trafficking disruptions or Ca^{2+}-induced mitochondrial swelling could interrupt mitochondrial function resulting in pathology. Alternatively, the various mutations could affect the same pathway but just at different stages. A disruption in this hypothetical pathway would then cause the subsequent pathogenesis of CNM. A potential way to improve the current understanding of the pathogenesis of CNM could be to improve Ca^{2+} sequestration in other models of CNM. Although PV^{OE} did not appear to improve CNM severity in this research project, other research has shown that overexpressing SERCA can improve the myopathy progression in *mdx* mice (Goonasekera et al., 2011). Because SERCA overexpression has improved other myopathies, overexpressing SERCA may improve the severity of CNM disease models. Overexpressing SERCA in PLN^{OE} mice would be redundant because it would only improve the ratio of SERCA to PLN resulting in less inhibited SR Ca^{2+}uptake. This has already been proven to work by administering a drug which would relieve PLN inhibition on SERCA (Reitze, unpublished). Instead, SERCA overexpression could be included in a CNM model originating from a dysfunctional membrane trafficking protein. If SERCA overexpression does not improve CNM in this theorized model then, it is possible that the pathogenesis occurs through Ca^{2+} independent pathways. However, if SERCA overexpression does improve the disease this could mean that elevated $[Ca^{2+}]_i$ is responsible for the progression of this disease. Regardless of the outcome, a transgenic model such as the one described would improve the understanding of the origins of CNM.

This thesis found that the overexpression of PV does not attenuate CNM brought on by PLN overexpression. However, other evidence still suggests Ca^{2+} is involved with the progression of CNM. Exploring the role of Ca^{2+} handling and signaling can further our understanding of the development of CNM while also contributing foundational knowledge to our understanding of the underlying cellular machinery within the myocyte.

References

Alderton, J. M., & Steinhardt, R. A. (2000). How calcium influx through calcium leak channels is responsible for the elevated levels of calcium-dependent proteolysis in dystrophic myotubes. *Trends in Cardiovascular Medicine*, *10*(6), 268–272. https://doi.org/10.1016/S1050-1738(00)00075-X

Alonso, A., Sasin, J., Bottini, N., Friedberg, I., Friedberg, I., Osterman, A., Godzik, A., Hunter, T., Dixon, J., & Mustelin, T. (2004). Protein tyrosine phosphatases in the human genome. *Cell*, *117*(6), 699–711. https://doi.org/10.1016/j.cell.2004.05.018

Anderson, D. M., Anderson, K. M., Chang, C., Makarewich, C. A., Nelson, B. R., Mcanally, J. R., Kasaragod, P., Shelton, J. M., Liou, J., Bassel-duby, R., & Olson, E. N. (2016). *A Micropeptide Encoded by a Putative Long Non-coding RNA Regulates Muscle Performance*. *160*(4), 595–606. https://doi.org/10.1016/j.cell.2015.01.009.A

Asahi, M., Kurzydlowski, K., Tada, M., & MacLennan, D. H. (2002). Sarcolipin inhibits polymerization of phospholamban to induce superinhibition of sarco(endo)plasmic reticulum Ca2+-ATPases (SERCAs). *Journal of Biological Chemistry*, *277*(30), 26725–26728. https://doi.org/10.1074/jbc.C200269200

Asahi, M., Sugita, Y., Kurzydlowski, K., De Leon, S., Tada, M., Toyoshima, C., & MacLennan, D. H. (2003). Sarcolipin regulates sarco(endo)plasmic reticulum Ca2+-ATPase (SERCA) by binding to transmembrane helices alone or in association with phospholamban. *Proceedings of the National Academy of Sciences of the United States of America*, *100*(9), 5040–5045. https://doi.org/10.1073/pnas.0330962100

Bárány, M., & Close, R. I. (1971). The transformation of myosin in cross-innervated rat muscles. *The Journal of Physiology*, *213*(2), 455–474. https://doi.org/10.1113/jphysiol.1971.sp009393

Baylor, S. M., & Hollingworth, S. (2003). Sarcoplasmic reticulum calcium release compared in slow-twitch and fast-twitch fibres of mouse muscle. *Journal of Physiology*, *551*(1), 125–138. https://doi.org/10.1113/jphysiol.2003.041608

Berridge, M. J., Lipp, P., & Bootman, M. D. (2000). 2000-Review-Calcium Signalling. *Nature Reviews*, *1*(October), 11–21.

Bevilacqua, J. A., Monnier, N., Bitoun, M., Eymard, B., Ferreiro, A., Monges, S., Lubieniecki, F., Taratuto, A. L., Laquerrière, A., Claeys, K. G., Marty, I., Fardeau, M., Guicheney, P., Lunardi, J., & Romero, N. B. (2011). Recessive RYR1 mutations cause unusual congenital myopathy with prominent nuclear internalization and large areas of myofibrillar disorganization. *Neuropathology and Applied Neurobiology*, *37*(3), 271–284. https://doi.org/10.1111/j.1365-2990.2010.01149.x

Bloemberg, D., & Quadrilatero, J. (2012). Rapid determination of myosin heavy chain expression in rat, mouse, and human skeletal muscle using multicolor immunofluorescence analysis. *PLoS ONE*, *7*(4). https://doi.org/10.1371/journal.pone.0035273

Blondeau, F., Laporte, J., Bodin, S., Superti-Furga, G., Payrastre, B., & Mandel, J. L. (2000). Myotubularin, a phosphatase deficient in myotubular myopathy, acts on phosphatidylinositol 3-kinase and phosphatidylinositol 3-phosphate pathway. *Human Molecular Genetics*, *9*(15), 2223–2229. https://doi.org/10.1093/oxfordjournals.hmg.a018913

Brandl, C. J., deLeon, S., Martin, D. R., & MacLennan, D. H. (1987). Adult forms of the

Ca2+ATPase of sarcoplasmic reticulum. Expression in developing skeletal muscle. *Journal of Biological Chemistry*, *262*(8), 3768–3774. https://doi.org/10.1016/s0021-9258(18)61421-8

Brandl, C. J., Green, N. M., Korczak, B., & MacLennan, D. H. (1986). Two Ca2+ ATPase genes: Homologies and mechanistic implications of deduced amino acid sequences. *Cell*, *44*(4), 597–607. https://doi.org/10.1016/0092-8674(86)90269-2

Burnham, R., Martin, T., Stein, R., Bell, G., MacLean, I., & Steadward, R. (1997). Skeletal muscle fibre type transformation following spinal cord injury. *Spinal Cord*, *35*(2), 86–91. https://doi.org/10.1038/sj.sc.3100364

Butera, G., Vecellio Reane, D., Canato, M., Pietrangelo, L., Boncompagni, S., Protasi, F., Rizzuto, R., Reggiani, C., & Raffaello, A. (2021). Parvalbumin affects skeletal muscle trophism through modulation of mitochondrial calcium uptake. *Cell Reports*, *35*(5), 109087. https://doi.org/10.1016/j.celrep.2021.109087

Caiozzo, V. J., Baker, M. J., Herrick, R. E., Tao, M., & Baldwin, K. M. (1994). Effect of spaceflight on skeletal muscle: Mechanical properties and myosin isoform content of a slow muscle. *Journal of Applied Physiology*, *76*(4), 1764–1773. https://doi.org/10.1152/jappl.1994.76.4.1764

Calabria, E., Ciciliot, S., Moretti, I., Garcia, M., Picard, A., Dyar, K. A., Pallafacchina, G., Tothova, J., Schiaffino, S., & Murgia, M. (2009). NFAT isoforms control activity-dependent muscle fiber type specification. *Proceedings of the National Academy of Sciences of the United States of America*, *106*(32), 13335–13340. https://doi.org/10.1073/pnas.0812911106

Calderón, J. C., Bolaños, P., & Caputo, C. (2014). The excitation-contraction coupling mechanism in skeletal muscle. *Biophysical Reviews*, *6*(1), 133–160. https://doi.org/10.1007/s12551-013-0135-x

Caldwell, J. L., Smith, C. E. R., Taylor, R. F., Kitmitto, A., Eisner, D. A., Dibb, K. M., & Trafford, A. W. (2014). Dependence of cardiac transverse tubules on the BAR domain protein amphiphysin II (BIN-1). *Circulation Research*, *115*(12), 986–996. https://doi.org/10.1161/CIRCRESAHA.116.303448

Carafoli, E., & Krebs, J. (2016). Why calcium? How calcium became the best communicator. *Journal of Biological Chemistry*, *291*(40), 20849–20857. https://doi.org/10.1074/jbc.R116.735894

Carnwath, J. W., & Shotton, D. M. (1987). Muscular dystrophy in the mdx mouse: Histopathology of the soleus and extensor digitorum longus muscles. *Journal of the Neurological Sciences*, *80*(1), 39–54. https://doi.org/10.1016/0022-510X(87)90219-X

Carpenter, C. E. (2001). Calcineurin-mediated signaling in skeletal muscle. *Canadian Journal of Animal Science*, *81*(3), 307–314. https://doi.org/10.4141/A01-023

Ceyhan-Birsoy, O., Agrawal, P. B., Hidalgo, C., Schmitz-Abe, K., Dechene, E. T., Swanson, L. C., Soemedi, R., Vasli, N., Iannaccone, S. T., Shieh, P. B., Shur, N., Dennison, J. M., Lawlor, M. W., Laporte, J., Markianos, K., Fairbrother, W. G., Granzier, H., & Beggs, A. H. (2013). Recessive truncating titin gene, TTN, mutations presenting as centronuclear myopathy. *Neurology*, *81*(14), 1205–1214. https://doi.org/10.1212/WNL.0b013e3182a6ca62

Chakkalakal, J. V., Stocksley, M. A., Harrison, M. A., Angus, L. M., Deschênes-Furry, J., St-Pierre, S., Megeney, L. A., Chin, E. R., Michel, R. N., & Jasmin, B. J. (2003). Expression of utrophin A mRNA correlates with the oxidative capacity of skeletal muscle fiber types and

is regulated by calcineurin/NFAT signaling. *Proceedings of the National Academy of Sciences of the United States of America*, *100*(13), 7791–7796. https://doi.org/10.1073/pnas.0932671100

Chambers, P. J. (n.d.). *The Effects of a Calcineurin Inhibitor on Muscle Fibre Type and the Pathology of Centronuclear Myopathy in PlnOE Mice*.

Chen, G., Carroll, S., Racay, P., Dick, J., Pette, D., Traub, I., Vrbova, G., Eggli, P., Celio, M., & Schwaller, B. (2001). Deficiency in parvalbumin increases fatigue resistance in fast-twitch muscle and upregulates mitochondria. *American Journal of Physiology - Cell Physiology*, *281*(1 50-1), 114–122. https://doi.org/10.1152/ajpcell.2001.281.1.c114

Chen, Z., Akin, B. L., & Jones, L. R. (2007). Mechanism of reversal of phospholamban inhibition of the cardiac Ca 2+-ATPase by protein kinase A and by anti-phospholamban monoclonal antibody 2D12. *Journal of Biological Chemistry*, *282*(29), 20968–20976. https://doi.org/10.1074/jbc.M703516200

Chin, E. R., Grange, R. W., Viau, F., Simard, A. R., Humphries, C., Shelton, J., Bassel-Duby, R., Williams, R. S., & Michel, R. N. (2003). Alterations in slow-twitch muscle phenotype in transgenic mice overexpressing the Ca2+ buffering protein parvalbumin. *Journal of Physiology*, *547*(2), 649–663. https://doi.org/10.1113/jphysiol.2002.024760

Chin, E. R., Olson, E. N., Richardson, J. A., Yang, Q., Humphries, C., Shelton, J. M., Wu, H., Zhu, W., Bassel-Duby, R., & Williams, R. S. (1998). A calcineurin-dependent transcriptional pathway controls skeletal muscle fiber type. *Genes and Development*, *12*(16), 2499–2509. https://doi.org/10.1101/gad.12.16.2499

Collet, C., Allard, B., Tourneur, Y., & Jacquemond, V. (1999). Intracellular calcium signals measured with indo-1 in isolated skeletal muscle fibres from control and mdx mice. *Journal of Physiology*, *520*(2), 417–429. https://doi.org/10.1111/j.1469-7793.1999.00417.x

Condon, K., Silberstein, L., Blau, H. M., & Thompson, W. J. (1990). Differentiation of fiber types in aneural musculature of the prenatal rat hindlimb. *Developmental Biology*, *138*(2), 275–295. https://doi.org/10.1016/0012-1606(90)90197-Q

Cowling, B. S., Chevremont, T., Prokic, I., Kretz, C., Ferry, A., Coirault, C., Koutsopoulos, O., Laugel, V., Romero, N. B., & Laporte, J. (2014). Reducing dynamin 2 expression rescues X-linked centronuclear myopathy. *Journal of Clinical Investigation*, *124*(3), 1350–1363. https://doi.org/10.1172/JCI71206

Cowling, B. S., Prokic, I., Tasfaout, H., Rabai, A., Humbert, F., Rinaldi, B., Nicot, A. S., Kretz, C., Friant, S., Roux, A., & Laporte, J. (2017). Amphiphysin (BIN1) negatively regulates dynamin 2 for normal muscle maturation. *Journal of Clinical Investigation*, *127*(12), 4477–4487. https://doi.org/10.1172/JCI90542

Cowling, B. S., Toussaint, A., Muller, J., & Laporte, J. (2012). Defective membrane remodeling in neuromuscular diseases: Insights from animal models. *PLoS Genetics*, *8*(4). https://doi.org/10.1371/journal.pgen.1002595

Crabtree, G. R., & Olson, E. N. (2002). NFAT signaling: Choreographing the social lives of cells. *Cell*, *109*(2 SUPPL. 1), 67–79. https://doi.org/10.1016/S0092-8674(02)00699-2

Damiani, E., Sacchetto, R., & Margreth, A. (2000). Variation of phospholamban in slow-twitch muscle sarcoplasmic reticulum between mammalian species and a link to the substrate specificity of endogenous Ca2+-calmodulin-dependent protein kinase. *Biochimica et Biophysica Acta - Biomembranes*, *1464*(2), 231–241. https://doi.org/10.1016/S0005-2736(00)00153-X

Degens, H., Meessen, N. E. L., Wirtz, P., & Binkhorst, R. A. (1995). The development of

compensatory hypertrophy in the plantaris muscle of the rat. *Annals of Anatomy*, *177*(3), 285–289. https://doi.org/10.1016/S0940-9602(11)80203-7

Dremina, E. S., Sharov, V. S., Davies, M. J., & Schöneich, C. (2007). Oxidation and inactivation of SERCA by selective reaction of cysteine residues with amino acid peroxides. *Chemical Research in Toxicology*, *20*(10), 1462–1469. https://doi.org/10.1021/tx700108w

Duhamel, T. A., Green, H. J., Stewart, R. D., Foley, K. P., Smith, I. C., & Ouyang, J. (2007). Muscle metabolic, SR Ca2+-cycling responses to prolonged cycling, with and without glucose supplementation. *Journal of Applied Physiology*, *103*(6), 1986–1998. https://doi.org/10.1152/japplphysiol.01440.2006

Dulhunty, A. F. (2006). Excitation-contraction coupling from the 1950s into the new millennium. *Clinical and Experimental Pharmacology and Physiology*, *33*(9), 763–772. https://doi.org/10.1111/j.1440-1681.2006.04441.x

Dunn, S. E., Burns, J. L., & Michel, R. N. (1999). Calcineurin is required for skeletal muscle hypertrophy. *Journal of Biological Chemistry*, *274*(31), 21908–21912. https://doi.org/10.1074/jbc.274.31.21908

Ecob-Prince, M. S., & Leberer, E. (1989). Parvalbumin in mouse muscle in vivo and in vitro. *Differentiation*, *40*(1), 10–16. https://doi.org/10.1111/j.1432-0436.1989.tb00808.x

Ehlers, M., Celona, B., & Black, B. (2014). *NFATc1 controls skeletal muscle fiber type and is a negative regulator of MyoD activity*. *8*(6), 1639–1648. https://doi.org/10.1016/j.celrep.2014.08.035.NFATc1

Fajardo, V. A., Bombardier, E., McMillan, E., Tran, K., Wadsworth, B. J., Gamu, D., Hopf, A., Vigna, C., Smith, I. C., Bellissimo, C., Michel, R. N., Tarnopolsky, M. A., Quadrilatero, J., & Tupling, A. R. (2015). Phospholamban overexpression in mice causes a centronuclear myopathy-like phenotype. *DMM Disease Models and Mechanisms*, *8*(8), 999–1009. https://doi.org/10.1242/dmm.020859

Fajardo, V. A., Bombardier, E., Vigna, C., Devji, T., Bloemberg, D., Gamu, D., Gramolini, A. O., Quadrilatero, J., & Tupling, A. R. (2013). Co-Expression of SERCA isoforms, phospholamban and sarcolipin in human skeletal muscle fibers. *PLoS ONE*, *8*(12), 1–13. https://doi.org/10.1371/journal.pone.0084304

Fajardo, V. A., Gamu, D., Mitchell, A., Bloemberg, D., Bombardier, E., Chambers, P. J., Bellissimo, C., Quadrilatero, J., & Russell Tupling, A. (2017). Sarcolipin deletion exacerbates soleus muscle atrophy and weakness in phospholamban overexpressing mice. *PLoS ONE*, *12*(3), 1–17. https://doi.org/10.1371/journal.pone.0173708

Fajardo, V. A., Smith, I. C., Bombardier, E., Chambers, P. J., Quadrilatero, J., & Tupling, A. R. (2016). Diaphragm assessment in mice overexpressing phospholamban in slow-twitch type I muscle fibers. *Brain and Behavior*, *6*(6), 1–10. https://doi.org/10.1002/brb3.470

Fohr, U. G., Weber, B. R., Muntener, M., Staudenmann, W., Hughes, G. J., Frutiger, S., Banville, D., Schafer, B. W., & Heizmann, C. W. (1993). Human alpha and beta parvalbumins. Structure and tissue-specific expression. *Eur J Biochem*, *215*(3), 719–727.

Folker, E. S., & Baylies, M. K. (2013). Nuclear positioning in muscle development and disease. *Frontiers in Physiology*, *4 DEC*(December), 1–10. https://doi.org/10.3389/fphys.2013.00363

Fraysse, B., Guicheneu, P., & Bitoun, M. (2016). Calcium homeostasis alterations in a mouse model of the dynamin 2-related centronuclear myopathy. *Biology Open*, *5*(11), 1691–1696. https://doi.org/10.1242/bio.020263

Fuchtbauer, E. M., Rowlerson, A. M., Gotz, K., Friedrich, G., Mabuchi, K., Gergely, J., &

Jockusch, H. (1991). Direct correlation of parvalbumin levels with myosin isoforms and succinate dehydrogenase activity on frozen sections of rodent muscle. *Journal of Histochemistry and Cytochemistry*, *39*(3), 355–361. https://doi.org/10.1177/39.3.1825216

González-Jamett, A. M., Momboisse, F., Haro-Acuña, V., Bevilacqua, J. A., Caviedes, P., & Cárdenas, A. M. (2013). Dynamin-2 function and dysfunction along the secretory pathway. *Frontiers in Endocrinology*, *4*(SEP), 1–9. https://doi.org/10.3389/fendo.2013.00126

Goonasekera, S. A., Lam, C. K., Millay, D. P., Sargent, M. A., Hajjar, R. J., Kranias, E. G., & Molkentin, J. D. (2011). Mitigation of muscular dystrophy in mice by SERCA overexpression in skeletal muscle. *Journal of Clinical Investigation*, *121*(3), 1044–1052. https://doi.org/10.1172/JCI43844

Gordon, A. M., Regnier, M., & Homsher, E. (2001). Skeletal and cardiac muscle contractile activation: Tropomyosin "rocks and rolls." *News in Physiological Sciences*, *16*(2), 49–55. https://doi.org/10.1152/physiologyonline.2001.16.2.49

Gorski, P. A., Glaves, J. P., Vangheluwe, P., & Young, H. S. (2013). Sarco(endo)plasmic reticulum calcium ATPase (SERCA) inhibition by sarcolipin is encoded in its luminal tail. *Journal of Biological Chemistry*, *288*(12), 8456–8467. https://doi.org/10.1074/jbc.M112.446161

Gorski, P. A., Trieber, C. A., Ashrafi, G., & Young, H. S. (2015). Regulation of the sarcoplasmic reticulum calcium pump by divergent phospholamban isoforms in zebrafish. *Journal of Biological Chemistry*, *290*(11), 6777–6788. https://doi.org/10.1074/jbc.M114.585604

Green, H. J., & Pette, D. (1997). Early metabolic adaptations of rabbit fast-twitch muscle to chronic low-frequency stimulation. *European Journal of Applied Physiology and Occupational Physiology*, *75*(5), 418–424. https://doi.org/10.1007/s004210050182

Grossman, E. J., Roy, R. R., Talmadge, R. J., Zhong, H., & Edgerton, V. R. (1998). Effects of inactivity on myosin heavy chain composition and size of rat soleus fibers. *Muscle & Nerve*, *21*(3), 375–389. https://doi.org/10.1002/(sici)1097-4598(199803)21:3<375::aid-mus12>3.3.co;2-y

Gundersen, K., Leberer, E., Lømo, T., Pette, D., & Staron, R. S. (1988). Fibre types, calcium-sequestering proteins and metabolic enzymes in denervated and chronically stimulated muscles of the rat. *The Journal of Physiology*, *398*(1), 177–189. https://doi.org/10.1113/jphysiol.1988.sp017037

Haiech, J., Derancourt, J., Pechère, J. F., & Demaille, J. G. (1979). Magnesium and Calcium Binding to Parvalbumins: Evidence for Differences between Parvalbumins and an Explanation of Their Relaxing Function. *Biochemistry*, *18*(13), 2752–2758. https://doi.org/10.1021/bi00580a010

Haviv, H., & Karlish, S. J. D. (2013). P-Type Pumps: Na+,K+-ATPase. In *Encyclopedia of Biological Chemistry: Second Edition* (2nd ed., Vol. 3). Elsevier Inc. https://doi.org/10.1016/B978-0-12-378630-2.00198-5

Heizmann, C. W. (1984). Parvalbumin, and intracellular calcium-binding protein; distribution, properties and possible roles in mammalian cells. *Experientia*, *40*(9), 910–921. https://doi.org/10.1007/BF01946439

Hennig, R., & Lomo, T. (1985). Firing Patterns of Motor Units in Normal Rats. *Nature*, *314*, 164–166.

Heskamp, L., Birkbeck, M. G., Whittaker, R. G., Schofield, I. S., & Blamire, A. M. (2021). The muscle twitch profile assessed with motor unit magnetic resonance imaging. *NMR in Biomedicine*, *34*(3), 1–15. https://doi.org/10.1002/nbm.4466

Hnia, K., Tronchère, H., Tomczak, K. K., Amoasii, L., Schultz, P., Beggs, A. H., Payrastre, B., Mandel, J. L., & Laporte, J. (2011). Myotubularin controls desmin intermediate filament architecture and mitochondrial dynamics in human and mouse skeletal muscle. *Journal of Clinical Investigation*, *121*(1), 70–85. https://doi.org/10.1172/JCI44021

Ho, S. N., Thomas, D. J., Timmerman, L. A., Li, X., Francke, U., & Crabtree, G. R. (1995). NFATc3, a lymphoid-specific NFATc family member that is calcium-regulated and exhibits distinct DNA binding specificity. In *Journal of Biological Chemistry* (Vol. 270, Issue 34, pp. 19898–19907). https://doi.org/10.1074/jbc.270.34.19898

Holmes, K. C. (2008). Chapter 2 Myosin Structure. *Myosins: A Superfamily of Molecular Motors*, 35–54.

Hopf, F. W., Turner, P. R., & Steinhardt, R. A. (2007). Calcium misregulation and the pathogenesis of muscular dystrophy. *Subcellular Biochemistry*, *45*, 429–464. https://doi.org/10.1007/978-1-4020-6191-2_16

Hou, T., Johnson, D., & Rall, J. A. (1991). EFFECT OF TEMPERATURE ON RELAXATION RATE AND Ca2+, Mg2+ DISSOCIATION RATES FROM PARVALBUMIN OF FROG MUSCLE FIBRES. *Journal of Physiology*, 399–410.

Hutter, M. C., Krebs, J., Meiler, J., Griesinger, C., Carafoli, E., & Helms, V. (2002). A structural model of the complex formed by phospholamban and the calcium pump of sarcoplasmic reticulum obtained by molecular mechanics. *ChemBioChem*, *3*(12), 1200–1208. https://doi.org/10.1002/1439-7633(20021202)3:12<1200::AID-CBIC1200>3.0.CO;2-H

Jungbluth, H., & Gautel, M. (2014). Pathogenic mechanisms in centronuclear myopathies. *Frontiers in Aging Neuroscience*, *6*(DEC), 1–11. https://doi.org/10.3389/fnagi.2014.00339

Jungbluth, H., Wallgren-Pettersson, C., & Laporte, J. (2008). Centronuclear (myotubular) myopathy. *Orphanet Journal of Rare Diseases*, *3*(1), 1–13. https://doi.org/10.1186/1750-1172-3-26

Klee, C. B., Crouch, T. H., & Krinks, M. H. (1979). Calcineurin: A calcium- and calmodulin-binding protein of the nervous system. *Proceedings of the National Academy of Sciences of the United States of America*, *76*(12), 6270–6273. https://doi.org/10.1073/pnas.76.12.6270

Kramerova, I., Kudryashova, E., Wu, B., Ottenheijm, C., Granzier, H., & Spencer, M. J. (2008). Novel role of calpain-3 in the triad-associated protein complex regulating calcium release in skeletal muscle. *Human Molecular Genetics*, *17*(21), 3271–3280. https://doi.org/10.1093/hmg/ddn223

Kranias, E. G., & Hajjar, R. J. (2012). Modulation of cardiac contractility by the phopholamban/SERCA2a regulatome. *Circulation Research*, *110*(12), 1646–1660. https://doi.org/10.1161/CIRCRESAHA.111.259754

Kretsinger, R. H., & Nockolds, C. E. (1973). Carp Muscle Calcium-binding Protein. *The Journal of Biological Chemistry*, *218*(9), 3313–3326.

Kutchukian, C., Szentesi, P., Allard, B., Buj-bello, A., Jacquemond, V., Kutchukian, C., Szentesi, P., Allard, B., Buj-bello, A., & Csernoch, L. (2019). Ca2 + -induced sarcoplasmic reticulum Ca2 + release in myotubularin-deficient muscle fibers To cite this version : HAL Id : hal-02325585. *Cell Calcium, Elsevier*, *80*, 91–100. https://doi.org/10.1016/j.ceca.2019.04.004

Lee, S. H., Schwaller, B., & Neher, E. (2000). Kinetics of Ca2+ binding to parvalbumin in bovine chromaffin cells: Implications for [Ca2+] transients of neuronal dendrites. *Journal of Physiology*, *525*(2), 419–432. https://doi.org/10.1111/j.1469-7793.2000.t01-2-00419.x

Lemasters, J. J., Theruvath, T. P., Zhong, Z., & Nieminen, A. L. (2009). Mitochondrial calcium

and the permeability transition in cell death. *Biochimica et Biophysica Acta - Bioenergetics*, *1787*(11), 1395–1401. https://doi.org/10.1016/j.bbabio.2009.06.009

Lichvarova, L., Henzi, T., Safiulina, D., Kaasik, A., & Schwaller, B. (2018). Parvalbumin alters mitochondrial dynamics and affects cell morphology. *Cellular and Molecular Life Sciences*, *75*(24), 4643–4666. https://doi.org/10.1007/s00018-018-2921-x

MacLennan, D. H., Brandl, C. J., Korczak, B., & Green, N. M. (1985). Amino-acid Sequence of a Ca2+ + Mg2+ - dependent ATPase from rabbit muscle sarcoplasmic reticulum, deduced from its complementary DNA sequence. *Nature*, *316*(22), 696–700.

MacLennan, D. H., & Kranias, E. G. (2003). Phospholamban: A crucial regulator of cardiac contractility. *Nature Reviews Molecular Cell Biology*, *4*(7), 566–577. https://doi.org/10.1038/nrm1151

Makarewich, C. A., Munir, A. Z., Schiattarella, G. G., Bezprozvannaya, S., Raguimova, O. N., Cho, E. E., Vidal, A. H., Robia, S. L., Bassel-Duby, R., & Olson, E. N. (2018). The DWORF micropeptide enhances contractility and prevents heart failure in a mouse model of dilated cardiomyopathy. *ELife*, *7*, 1–23. https://doi.org/10.7554/eLife.38319

Mann, C. J., Perdiguero, E., Kharraz, Y., Aguilar, S., Pessina, P., Serrano, A. L., & Muñoz-Cánoves, P. (2011). Aberrant repair and fibrosis development in skeletal muscle. *Skeletal Muscle*, *1*(1), 1–20. https://doi.org/10.1186/2044-5040-1-21

McCullagh, K. J. A., Calabria, E., Pallafacchina, G., Ciciliot, S., Serrano, A. L., Argentini, C., Kalhovde, J. M., Lømo, T., & Schiaffino, S. (2004). NFAT is a nerve activity sensor in skeletal muscle and controls activity-dependent myosin switching. *Proceedings of the National Academy of Sciences of the United States of America*, *101*(29), 10590–10595. https://doi.org/10.1073/pnas.0308035101

McDonald, A. A., Hebert, S. L., Kunz, M. D., Ralles, S. J., & McLoon, L. K. (2015). Disease course in mdx:Utrophin+/− mice: comparison of three mouse models of duchenne muscular dystrophy. *Physiological Reports*, *3*(4), 1–22. https://doi.org/10.14814/phy2.12391

Minamisawa, S., Wang, Y., Chen, J., Ishikawa, Y., Chien, K. R., & Matsuoka, R. (2003). Atrial chamber-specific expression of sarcolipin is regulated during development and hypertrophic remodeling. *Journal of Biological Chemistry*, *278*(11), 9570–9575. https://doi.org/10.1074/jbc.M213132200

Mundiña Weilenmann, C., Ferrero, P., Said, M., Vittone, L., Kranias, E. G., & Mattiazzi, A. (2005). Role of phosphorylation of Thr17 residue of phospholamban in mechanical recovery during hypercapnic acidosis. *Cardiovascular Research*, *66*(1), 114–122. https://doi.org/10.1016/j.cardiores.2004.12.028

Müntener, M., Käser, L., Weber, J., & Berchtold, M. W. (1995). Increase of skeletal muscle relaxation speed by direct injection of parvalbumin cDNA. *Proceedings of the National Academy of Sciences of the United States of America*, *92*(14), 6504–6508. https://doi.org/10.1073/pnas.92.14.6504

Musarò, A., McCullagh, K. J. A., Naya, F. J., Olson, E. N., & Rosenthal, N. (1999). IGF-1 induces skeletal myocyte hypertrophy through calcineurin in association with GATA-2 and NF-ATc1. *Nature*, *400*(6744), 581–585. https://doi.org/10.1038/23060

Naya, F. J., Mercer, B., Shelton, J., Richardson, J. A., Williams, R. S., & Olson, E. N. (2000). Stimulation of slow skeletal muscle fiber gene expression by calcineurin in vivo. *Journal of Biological Chemistry*, *275*(7), 4545–4548. https://doi.org/10.1074/jbc.275.7.4545

Parsons, S. A., Milla, D. P., Wilkins, B. J., Bueno, O. F., Tsika, G. L., Neilson, J. R., Liberatore, C. M., Yutzey, K. E., Crabtree, G. R., Tsika, R. W., & Molkentin, J. D. (2004). Genetic loss

of calcineurin blocks mechanical overload-induced skeletal muscle fiber type switching but not hypertrophy. *Journal of Biological Chemistry*, *279*(25), 26192–26200. https://doi.org/10.1074/jbc.M313800200

Pattison, J. S., Waggoner, J. R., James, J., Martin, L., Gulick, J., Osinska, H., Klevitsky, R., Kranias, E. G., & Robbins, J. (2008). Phospholamban Overexpression in Transgenic Rabbits. *Transgenic Research*, *17*(2), 157–170. file:///Users/mayyungtiet/Documents/My work/PhD/Projects/Other projects/Leigh treatabolome/Review papers/Review references MT/Gempel 2007 ETFGDH.pdf

Pattullo, M., Cotter, M., Cameron, N., & Barry, J. (1992). Effects of lengthened immobilization on functional and histochemical properties of rabbit tibialis anterior muscle. *Experimental Physiology*, *77*(3), 433–442. https://doi.org/10.1113/expphysiol.1992.sp003604

Periasamy, M., & Kalyanasundaram, A. (2007). SERCA pump isoforms: Their role in calcium transport and disease. *Muscle and Nerve*, *35*(4), 430–442. https://doi.org/10.1002/mus.20745

Pette, D., & Staron, R. S. (1997). Mammalian skeletal muscle fiber type transitions. *International Review of Cytology*, *170*, 143–223. https://doi.org/10.1016/s0074-7696(08)61622-8

Praefcke, G. J. K., & McMahon, H. T. (2004). The dynamin superfamily: Universal membrane tubulation and fission molecules? *Nature Reviews Molecular Cell Biology*, *5*(2), 133–147. https://doi.org/10.1038/nrm1313

Prokic, I., Cowling, B. S., & Laporte, J. (2014). Amphiphysin 2 (BIN1) in physiology and diseases. *Journal of Molecular Medicine*, *92*(5), 453–463. https://doi.org/10.1007/s00109-014-1138-1

Racay, P., Gregory, P., & Schwaller, B. (2006). Parvalbumin deficiency in fast-twitch muscles leads to increased "slow-twitch type" mitochondria, but does not affect the expression of fiber specific proteins. *FEBS Journal*, *273*(1), 96–108. https://doi.org/10.1111/j.1742-4658.2005.05046.x

Rao, A., Luo, C., & Hogan, P. G. (1997). Transcription factors of the NFAT family: Regulation and function. *Annual Review of Immunology*, *15*, 707–747. https://doi.org/10.1146/annurev.immunol.15.1.707

Rietze, B. A. (n.d.). *Formoterol improves a centronuclear myopathy like phenotype displayed in phospholamban over-expressing mice: A Current Report*.

Rizzuto, R., Simpson, A. W. M., Brini, M., & Pozzan, T. (1992). Rapid changes of mitochodrial Ca2+ revealed by specifically targeted recombinant aequorin. *Nature*, *359*, 710–713. file:///C:/Users/ASUS/Desktop/Rujukan PhD/p21/xiong1993.pdf

Romero, N. B., & Bitoun, M. (2011). Centronuclear Myopathies. *Seminars in Pediatric Neurology*, *18*(4), 250–256. https://doi.org/10.1016/j.spen.2011.10.006

Rumi-Masante, J., Rusinga, F. I., Lester, T. E., Dunlap, T. B., Williams, T. D., Dunker, A. K., Weis, D. D., & Creamer, T. P. (2012). Structural basis for activation of calcineurin by calmodulin. *Journal of Molecular Biology*, *415*(2), 307–317. https://doi.org/10.1016/j.jmb.2011.11.008

Salmons, B. Y. S., & Vrbova, G. (1969). *THE INFLUENCE OF ACTIVITY ON SOME CONTRACTILE CHARACTERISTICS OF MAMMALIAN FAST AND SLOW MUSCLES*. *201*, 535–549.

Sanvicens, N., Gómez-Vicente, V., Masip, I., Messeguer, A., & Cotter, T. G. (2004). Oxidative stress-induced apoptosis in retinal photoreceptor cells is mediated by calpains and caspases

and blocked by the oxygen radical scavenger CR-6. *Journal of Biological Chemistry*, *279*(38), 39268–39278. https://doi.org/10.1074/jbc.M402202200
Schiaffino, S., Gorza, L., Pitton, G., Saggin, L., Ausoni, S., Sartore, S., & Lømo, T. (1988). Embryonic and neonatal myosin heavy chain in denervated and paralyzed rat skeletal muscle. *Developmental Biology*, *127*(1), 1–11. https://doi.org/10.1016/0012-1606(88)90183-2
Schiaffino, S., & Reggiani, C. (1994). Myosin isoforms in mammalian skeletal muscle. *Journal of Applied Physiology*, *77*(2), 493–501. https://doi.org/10.1152/jappl.1994.77.2.493
Schiaffino, S., & Reggiani, C. (2011). Fiber types in Mammalian skeletal muscles. *Physiological Reviews*, *91*(4), 1447–1531. https://doi.org/10.1152/physrev.00031.2010
Schmidt, U., Zhu, X., Lebeche, D., Huq, F., Guerrero, J. L., & Hajjar, R. J. (2005). In vivo gene transfer of parvalbumin improves diastolic function in aged rat hearts. *Cardiovascular Research*, *66*(2), 318–323. https://doi.org/10.1016/j.cardiores.2004.06.028
Schmitt, J. P., Kamisago, M., Asahi, M., Hua Li, G., Ahmad, F., Mende, U., Kranias, E. G., MacLennan, D. H., Seidman, J. G., & Seidman, C. E. (2003). Dilated cardiomyopathy and heart failure caused by a mutation in phospholamban. *Science*, *299*(5611), 1410–1413. https://doi.org/10.1126/science.1081578
Schwaller, B., Dick, J., Dhoot, G., Carroll, S., Vrbova, G., Nicotera, P., Pette, D., Wyss, A., Bluethmann, H., Hunziker, W., & Celio, M. R. (1999). Prolonged contraction-relaxation cycle of fast-twitch muscles in parvalbumin knockout mice. *American Journal of Physiology - Cell Physiology*, *276*(2 45-2), 395–403. https://doi.org/10.1152/ajpcell.1999.276.2.c395
Scott, W., Stevens, J., & Binder-Macleod, S. A. (2001). Human skeletal muscle fiber type classifications. *Physical Therapy*, *81*(11), 1810–1816. https://doi.org/10.1093/ptj/81.11.1810
Serrano, A. L., Murgia, M., Pallafacchina, G., Calabria, E., Coniglio, P., Lømo, T., & Schiaffino, S. (2001). Calcineurin controls nerve activity-dependent specification of slow skeletal muscle fibers but not muscle growth. *Proceedings of the National Academy of Sciences of the United States of America*, *98*(23), 13108–13113. https://doi.org/10.1073/pnas.231148598
Shen, J., Yu, W., Brotto, M., Scherman, J. A., Guo, C., Stoddard, C., Nosek, T. M., Valdivia, H. H., & Qu, C. (2009). *Deficiency of MIP phosphatase induces a muscle disorder by disrupting Ca2+ homeostasis*. *11*(6), 769–776. https://doi.org/10.1038/ncb1884.Deficiency
Sher, J. H., Rimalovski, A. B., Athanassiades, T. J., & Aronson, S. M. (1967). *centronuclear myopathy: 17*(August).
Smeazzetto, S., Tadini-Buoninsegni, F., Thiel, G., Berti, D., & Montis, C. (2016). Phospholamban spontaneously reconstitutes into giant unilamellar vesicles where it generates a cation selective channel. *Physical Chemistry Chemical Physics*, *18*(3), 1629–1636. https://doi.org/10.1039/c5cp05893g
Smith, I. C. (2014). *The role of cytosolic calcium in potentiation of mouse lumbrical muscle*.
Sommer, J. R. (1982). The Anatomy of the Sarcoplasmic Reticulum in Vertebrate Skeletal Muscle: Its Implications for Excitation Contraction Coupling. *Zeitschrift Fur Naturforschung - Section C Journal of Biosciences*, *37*(7–8), 665–678. https://doi.org/10.1515/znc-1982-7-816
Song, Q., Young, K. B., Chu, G., Gulick, J., Gerst, M., Grupp, I. L., Robbins, J., & Kranias, E. G. (2004). Overexpression of phospholamban in slow-twitch skeletal muscle is associated

with depressed contractile function and muscle remodeling. *The FASEB Journal*, *18*(9), 1–19. https://doi.org/10.1096/fj.03-1058fje

Spiro, A. J., Shy, G. M., & Gonatas, N. K. (1966). Myotubular Myopathy: Persistence of Fetal Muscle in an Adolescent Boy. *Archives of Neurology*, *14*(1), 1–14. https://doi.org/10.1001/archneur.1966.00470070005001

Taylor., A. W., Essén, B., & Saltin, B. (1974). Myosin ATPase in Skeletal Muscle of Healthy Men. *Acta Physiologica Scandinavica*, *91*(4), 568–570. https://doi.org/10.1111/j.1748-1716.1974.tb05712.x

Termin, A., Staron, R. S., & Pette, D. (1989). Changes in myosin heavy chain isoforms during chronic low-frequency stimulation of rat fast hindlimb muscles: A single-fiber study. *European Journal of Biochemistry*, *186*(3), 749–754. https://doi.org/10.1111/j.1432-1033.1989.tb15269.x

Tinelli, E., Pereira, J. A., & Suter, U. (2013). Muscle-specific function of the centronuclear myopathy and charcot-marie-tooth neuropathyassociated dynamin 2 is required for proper lipid metabolism, mitochondria, muscle fibers, neuromuscular junctions and peripheral nerves. *Human Molecular Genetics*, *22*(21), 4417–4429. https://doi.org/10.1093/hmg/ddt292

Tosch, V., Rohde, H. M., Tronchère, H., Zanoteli, E., Monroy, N., Kretz, C., Dondaine, N., Payrastre, B., Mandel, J. L., & Laporte, J. (2006). A novel PtdIns3P and PtdIns(3,5)P2 phosphatase with an inactivating variant in centronuclear myopathy. *Human Molecular Genetics*, *15*(21), 3098–3106. https://doi.org/10.1093/hmg/ddl250

Toyoshima, C., Asahi, M., Sugita, Y., Khanna, R., Tsuda, T., & MacLennan, D. H. (2003). Modeling of the inhibitory interaction of phospholamban with the Ca2+ ATPase. *Proceedings of the National Academy of Sciences of the United States of America*, *100*(2), 467–472. https://doi.org/10.1073/pnas.0237326100

Toyoshima, C., & Inesi, G. (2004). Structural basis of ion pumping by Ca2+-ATPase of the sarcoplasmic reticulum. *Annual Review of Biochemistry*, *73*, 269–292. https://doi.org/10.1146/annurev.biochem.73.011303.073700

Toyoshima, C., Nakasako, M., Nomura, H., & Ogawa, H. (2000). Crystal structure of the calcium pump of sarcoplasmic reticulum at 2.6 Å resolution. *Nature*, *405*(6787), 647–655. https://doi.org/10.1038/35015017

Vrbová, G. (1963). The effect of motoneurone activity on the speed of contraction of striated muscle. *The Journal of Physiology*, *169*(3), 513–526. https://doi.org/10.1113/jphysiol.1963.sp007276

Wang, W., Barnabei, M. S., Asp, M. L., Heinis, F. I., Arden, E., Davis, J., Braunlin, E., Li, Q., Davis, J. P., Potter, J. D., & Metzger, J. M. (2013). Noncanonical EF-hand motif strategically delays Ca2+ buffering to enhance cardiac performance. *Nature Medicine*, *19*(3), 305–312. https://doi.org/10.1038/nm.3079

Wegener, A. D., & Jones, L. R. (1984). Phosphorylation-induced mobility shift in phospholamban in sodium dodecyl sulfate-polyacrylamide gels. Evidence for a protein structure consisting of multiple identical phosphorylatable subunits. *Journal of Biological Chemistry*, *259*(3), 1834–1841. https://doi.org/10.1016/s0021-9258(17)43484-3

Wegener, A. D., Simmerman, H. K. B., Lindemann, J. P., & Jones, L. R. (1989). Phospholamban phosphorylation in intact ventricles. Phosphorylation of serine 16 and threonine 17 in response to β-adrenergic stimulation. *Journal of Biological Chemistry*, *264*(19), 11468–11474. https://doi.org/10.1016/S0021-9258(18)60487-9

Westerblad, H., & Allen, D. G. (1993). The contribution of [Ca2+]i to the slowing of relaxation in fatigued single fibres from mouse skeletal muscle. *The Journal of Physiology*, *468*(1), 729–740. https://doi.org/10.1113/jphysiol.1993.sp019797

Whitehead, N. P., Yeung, E. W., & Allen, D. G. (2006). Muscle damage in mdx (dystrophic) mice: Role of calcium and reactive oxygen species. *Clinical and Experimental Pharmacology and Physiology*, *33*(7), 657–662. https://doi.org/10.1111/j.1440-1681.2006.04394.x

Wilmshurst, J. M., Lillis, S., Zhou, H., Pillay, K., Henderson, H., Kress, W., Müller, C. R., Ndondo, A., Cloke, V., Cullup, T., Bertini, E., Boennemann, C., Straub, V., Quinlivan, R., Dowling, J. J., Al-Sarraj, S., Treves, S., Abbs, S., Manzur, A. Y., … Jungbluth, H. (2010). RYR1 mutations are a common cause of congenital myopathies with central nuclei. *Annals of Neurology*, *68*(5), 717–726. https://doi.org/10.1002/ana.22119

Wittmann, T., Lohse, M. J., & Schmitt, J. P. (2015). Phospholamban pentamers attenuate PKA-dependent phosphorylation of monomers. *Journal of Molecular and Cellular Cardiology*, *80*, 90–97. https://doi.org/10.1016/j.yjmcc.2014.12.020

Yang, S. A., & Klee, C. B. (2000). Low affinity Ca2+-binding sites of calcineurin B mediate conformational changes in calcineurin A. *Biochemistry*, *39*(51), 16147–16154. https://doi.org/10.1021/bi001321q

Zhou, H., Rokach, O., Feng, L., Munteanu, I., Mamchaoui, K., Wilmshurst, J. M., Sewry, C., Manzur, A. Y., Pillay, K., Mouly, V., Duchen, M., Jungbluth, H., Treves, S., & Muntoni, F. (2013). RyR1 Deficiency in Congenital Myopathies Disrupts Excitation-Contraction Coupling. *Human Mutation*, *34*(7), 986–996. https://doi.org/10.1002/humu.22326

Zhou, J., Dhakal, K., & Yi, J. (2011). Mitochondrial Ca2+ uptake in skeletal muscle health and disease. *Physiology & Behavior*, *176*(5), 139–148. https://doi.org/10.1007/s11427-016-5089-3.Mitochondrial

Appendix A

Genotyping Protocol

All PLN^{OE}/PV^{OE} mice were ear notched at 3-4 weeks. DNA was then digested with 1.0 mg/ml Proteinase K in Mouse Tail Isolation Buffer left overnight in a 63°C water bath. 37.6 ul of 8M potassium acetate and 250ul of chloroform were added to samples and vortexed for 10 mins. Samples were then centrifuged for 8 mins at 5000 rpm at room temperature. Following centrifugation the supernatant was isolated and 2 volumes of 100% ethanol was added. The DNA extracts were centrifuged again for 20 mins at 14000 rpm at 4°C. Supernatant was then removed and 30 uL of water was added. DNA concentrations of samples were quantified and normalized to 20 ng/uL.

Table 1: Genotyping Master Mix Solution

	Buffer	dNTP	Forward Primer	Reverse Primer	$MgCl_2$	Taq DNA Polymerase	H2O
PVHA	10x KCl Buffer 2.5 uL	0.5uL	TnIs-PVHA-B 0.5uL	TnIs-PVHA-A 0.5uL	5uL	0.125uL	13.875uL
PLN^{OE}	10x SO_4 Buffer 2.5 uL	0.5uL	SK-1 0.5uL	PLB-RC 0.5uL	5uL	0.125uL	14.875uL

PVHA PCR Protocol

Forward PVHA primer **Tnls-PVHA** 5'- TTA GGC GTA GTC GGG CAC GTC ATA TGG GTA GCT TTC GGC CAC CAG AGT GGA-3'

Reverse PVHA primer **Tnls-PVHA BamHI** 5'-CCC ACC AGC CCA GCT TTT CTA-3'

1. Denaturation: 95°C – 5 mins
2. Denaturation: 94°C – 30 secs
3. Annealing: 65°C – 30 secs
4. Extension: 72°C – 1 min

   Repeat steps 2 - 4 for 23 cycles
5. Final extension: 72°C – 10 mins
6. Hold at 4°C

Gel: 1.3 g agarose in 100 mL of 1x TBE

Electrophoresis: 70V for 35 mins

PLN^{OE} PCR Protocol

Forward PLN^{OE} primer, **SK-1**: 5'-AAG GGG CGG GAA GGC ATA TAG-3'

Reverse PLN^{OE} primer, **PLB-RC**: 5'-GAT TCT GAC GTG CTT GCT GAGG-3'

1. Denaturation: 95°C – 3 mins
2. Denaturation: 94°C – 30 secs
3. Annealing: 70°C – 30 secs
4. Extension: 72°C – 1 min

Repeat steps 2 - 4 for 34 cycles

5. Final extension: 72°C – 10 mins
6. Hold at 4°C

Gel: 1.3 g agarose in 100 mL of 1x TBE

Electrophoresis: 70V for 35 mins

Table 2: Western Blotting Protocol

Target Protein	Gel % (Type)	Membrane	Antibody Info	Primary	Secondary	Detection	Protein Weight
SERCA1a	7.5% (Glycine)	PVDF	A-52 Monoclonal Mouse	1:10000 in 5% 1 hr @ RT	1:20000 anti-mouse	Luminata 2 min exposure	110 kDa
SERCA2a	7.5% (Glycine)	PVDF	Invitrogen MA3-919 Monoclonal Mouse	1:2000 in 5% milk overnight 4°C	1:5000 anti-mouse	Luminata 2 min exposure	110 kDa (Bottom band)
PLN	13% (Tricine)	PVDF	Pierce Antibodies 2D12 Monoclonal Mouse	1:2000 signal enhancer 1 hr @ RT	1:2000 anti-mouse	Luminata 2 min exposure	6 kDa
PLN-p	13% (Tricine)	PVDF	Cell Signaling 8486S Polyclonal Rabbit	1:5000 in 3% BSA overnight 4°C	1:5000 anti-rabbit	Luminata 2 min exposure	6 kDa
CnA	7.5% (Glycine)	PVDF	Sigma Aldrich C1956 Monoclonal Mouse	1:1000 5% milk in TBST overnight 4°C	1:2000 anti-mouse	Femto 30 sec exposure	89 kDa
NFAT-p	7.5% (Glycine)	PVDF	Pierce Antibodies PA5-38301 Polyclonal Rabbit	1:2000 5% milk in TBST overnight 4°C	1:2000 anti-mouse	Luminata 2 min exposure	90 kDa
NFAT	7.5% (Glycine)	PVDF	Pierce Antibodies MA3-024 Monoclonal Mouse	1:2000 signal enhancer overnight 4°C	1:2000 anti-mouse	Luminata 2 min exposure	90 kDa
PV	13% (Tricine)	NC	SWant PVG 214 Goat	1:1000 in 5% milk overnight 4°C	1:2000 anti goat	Luminata 2 min exposure	PVHA – 16 kDa Endogenous PV - 14 kDa

Table 3: Antibodies for Immunohistochemistry

Target Protein	Antibody Info	Primary	Secondary
MHCI	BA-F8	1:50 1 hour incubation	AlexaFluor 350 anti-mouse IgG_{2b} Dilution: 1:500
MHCIIa	SC-71	1:600 1 hour incubation	AlexaFluor 488 anti-mouse IgG_1 Dilution: 1:500
MHCIIb	BF-F3	1:100 1 hour incubation	AlexaFluor 555 anti-mouse IgM Dilution: 1:500